Quinazoline-2-carboxamides as Selective PET Radiotracers for Matrix Metalloproteinase-13 Imaging in Atherosclerosis

Ariel Buchler,[1,2] Uzair S. Ismailani,[2,3] Nicole MacMullin,[2] Faduma Abdirahman,[1,2]

Myriam Adi,[1,2] Christina Bi,[1,2] Catherine Jany,[2] Jeffrey W. Keillor,[1] Benjamin H. Rotstein[1,2,3]*

[1] Department of Chemistry and Biomolecular Sciences, University of Ottawa, Ottawa, Ontario, K1N 9B4, Canada.

[2] University of Ottawa Heart Institute, Ottawa, Ontario, K1Y 4W7, Canada.

[3] Department of Biochemistry, Microbiology and Immunology, University of Ottawa, Ottawa, Ontario, K1H 8M5, Canada

Correspondence: Benjamin H. Rotstein, PhD
University of Ottawa Heart Institute
40 Ruskin Street, H-5219
Ottawa, Ontario, Canada
K1Y 4W7
Phone: 613-696-7324
Email: benjamin.rotstein@uottawa.ca

ABSTRACT

Matrix metalloproteinase-13 (MMP-13) plays a critical role in the progression of unstable atherosclerosis. A series of highly potent and selective MMP-13 inhibitors were synthesized around a quinazoline-2-carboxamide scaffold to facilitate radiolabeling with fluorine-18 or carbon-11 positron-emitting nuclides and visualization of atherosclerotic plaques. *In vitro* enzyme inhibition assays identified 3 compounds as promising radiotracer candidates. Efficient automated radiosyntheses provided **[^{11}C]5b**, **[^{11}C]5f** and **[^{18}F]5j** and enabled pharmacokinetic characterization in atherosclerotic mice. The radiotracers displayed substantial differences in their distribution and excretion. Most favourably for vascular imaging, **[^{18}F]5j** exhibited low uptake in metabolic organs with minimal retention of myocardial radioactivity, substantial renal clearance, and high metabolic stability in plasma. *Ex vivo* aortic autoradiography and competition studies revealed that **[^{18}F]5j** specifically binds to MMP-13 within atherosclerotic plaques and localizes to lipid-rich regions. This study demonstrates the utility of the quinazoline-2-carboxamide scaffold for MMP-13 selective PET radiotracer development and identifies **[^{18}F]5j** for imaging atherosclerosis.

Keywords

matrix metalloproteinase-13, positron emission tomography, radiotracer, atherosclerosis, extracellular matrix, collagenase, aortic autoradiography

INTRODUCTION

Matrix metalloproteinases (MMPs) represent a family of zinc-containing endopeptidases that play a critical role in embryonic development, cell migration, and tissue remodeling by degradation of extracellular matrix proteins.[1,2] Although the catalytic domain of MMPs is highly

conserved, these enzymes have several physiological roles and are classified based on their distinct substrate specificities and cellular localizations.[1–3] Typically, MMPs are secreted as zymogens whose activation is tightly controlled, while dysregulation of MMP activity is implicated in the pathogenesis of several inflammatory processes.[3–6] Given the functional diversity observed across the MMP family and their variable contribution to disease progression, selective targeting of individual MMPs is an advantageous approach for therapy and diagnosis.

MMP-13, also known as collagenase-3, is highly conserved among humans and mice and possesses substrate specificity for fibrillar collagen, a major component of the extracellular matrix that imparts biomechanical stability and tensile strength to connective tissues and vasculature.[7] Constitutive physiological expression of MMP-13 is restricted to skeletal tissue where it is secreted by chondrocytes and plays an important role in the development of growth plate cartilage and ossification.[8,9] Meanwhile, aberrant activation of MMP-13 is associated with the progression of osteoarthritis[10–12], breast cancer[13,14], and atherosclerosis.[15–18] Several preclinical studies have indicated that activation of MMP-13 within atherosclerotic plaques induces an unstable phenotype by decreasing fibrous cap thickness, reducing collagen content and organization, and hindering smooth muscle cell migration.[15,16] Densitometric analysis further revealed that MMP-13 was upregulated >5-fold in atheromatous compared with fibrous plaques and non-detectable in healthy arteries, supporting the potential for differentiation of stable and unstable forms of disease.[15] Additionally, deletion or selective inhibition of MMP-13 confers plaque stability.[17,18] Taken together, these findings suggest that this enzyme represents a potential *in vivo* biomarker for molecular imaging by positron emission tomography (PET) that contributes to pathology and could enable early detection of unstable plaques prior to rupture and prevent subsequent acute ischemic events.

Currently, atherosclerosis imaging is most commonly conducted using [^{18}F]FDG and [^{18}F]NaF to detect inflammation and microcalcification within the vasculature.[19,20] Vascular [^{18}F]FDG imaging is hampered by the relatively indiscriminate nature of its signal and significant non-specific uptake in other metabolically active cells such as the myocardium, which restricts its utility to the carotid arteries.[21] In contrast, the feasibility of detecting coronary artery atherosclerosis has been successfully demonstrated with [^{18}F]NaF and appears highly promising for identification of culprit plaques.[21] Previously developed MMP-targeted radiotracers, including [^{99m}Tc]RYM-1[22,23] and [^{18}F]BR-351,[24,25] and therapeutic agents such as marimastat[26] are based on hydroxamate-containing inhibitors that coordinate the active site zinc(II) ion, common to all MMPs. However, considering that many clinical trials using broad-spectrum MMP inhibitors have been discontinued due to the onset of musculoskeletal syndrome attributed to inhibition of non-pathological MMPs, there is a clear need for inhibitors with improved selectivity.[27–29] Substantial efforts toward this end have uncovered several highly potent small molecule MMP-13 inhibitors that retain significant selectivity by exploiting structural differences in binding pockets adjacent to the active site.[30–40] Among them, inhibitors based on pyrimidine-dicarboxamide and quinazoline-2-carboxamide scaffolds are promising candidates for radiotracer development as they possess reliable handles for radiolabeling with fluorine-18 or carbon-11.

Our group recently substantiated the feasibility of detecting inflammatory plaques in mouse models of atherosclerosis with an MMP-13 selective PET radiotracer ([^{18}F]FMBP) derived from the pyrimidine-dicarboxamide inhibitor class.[41] In this comparative evaluation, [^{18}F]FMBP exhibited substantially greater plaque uptake, improved sensitivity to atherosclerotic tissue, and displayed suitable specific binding relative to the aforementioned non-selective radiotracer, [^{18}F]BR-351. Nevertheless, significant challenges remain in quantifying atherosclerotic plaques

non-invasively due to retention of radioactivity in the myocardium and liver, requiring alternative MMP-13 targeted radiotracers with improved pharmacokinetics for vascular imaging.

Lead compounds based on these scaffolds achieve their target affinity through hydrogen bonding interactions between their central scaffolds and amino acid residues Ala238, Leu239, Thr245, Thr247, and Met253 found within the S_1' specificity pocket (Figure 1).[30,32] Both pyrimidine- and quinazoline-based MMP-13 inhibitors adopt a U-shaped binding mode anchored by *N*-benzylamides occupying a hydrophobic pocket formed by Phe241 and His222. Meanwhile, selectivity is further improved by occupying the distal S_1'' side pocket, which is not observed among other MMPs.[32] In particular, the lead quinazoline-2-carboxamide compound originally reported by Nara *et al*. (herein entitled **5b**) features a carboxylate that extends deeply within the S_1'' side pocket, forming additional hydrogen bonding and ionic interactions with Asn215 and Lys140 and represents the most potent and selective MMP-13 inhibitor reported to date.[32] Additionally, this compound is metabolically stable *in vitro*, and possesses favourable clearance profiles across various species. As of yet, no quinazoline-based MMP-13 inhibitors have been radiolabeled and evaluated as imaging agents.[32]

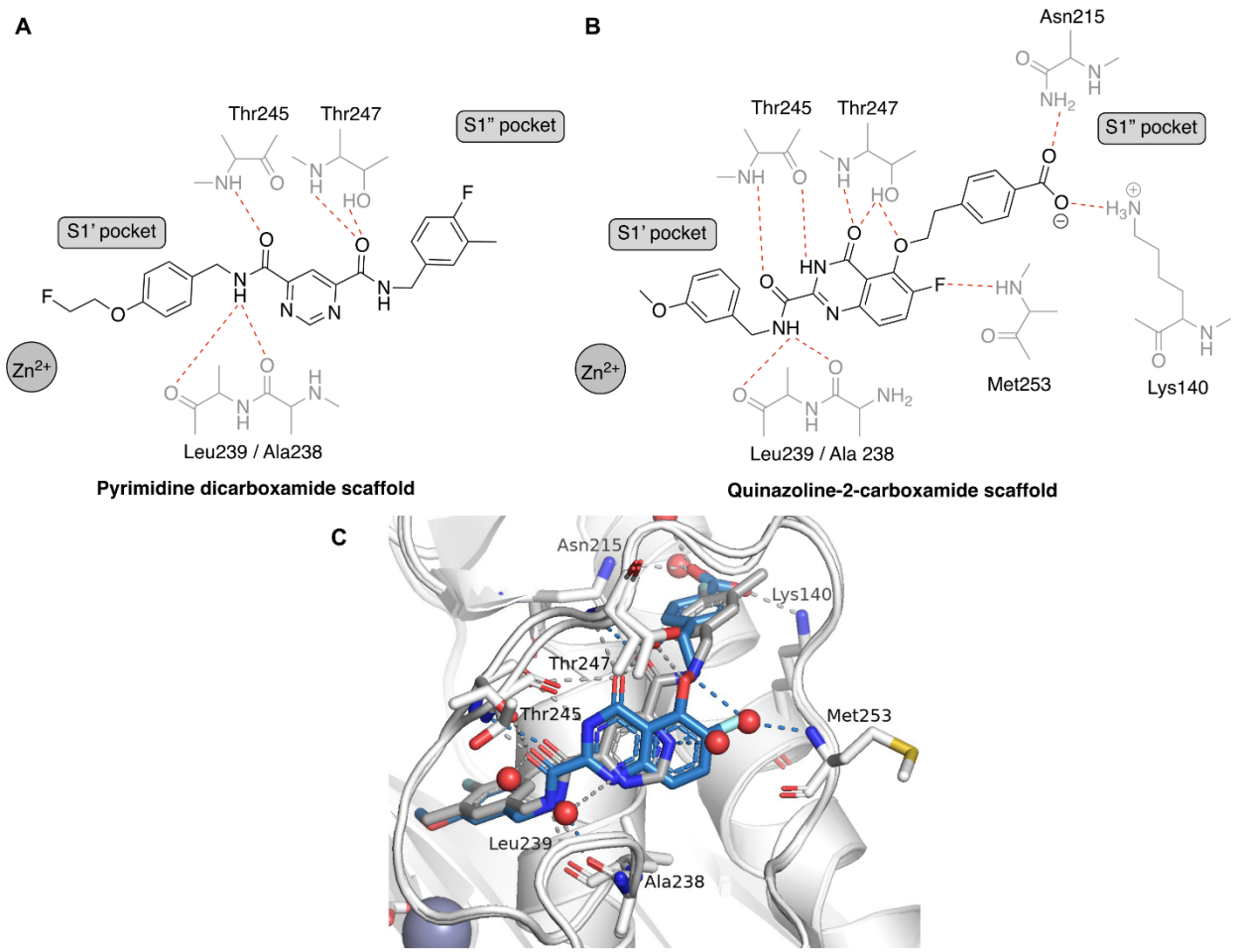

Figure 1. Putative binding mode of lead inhibitors with MMP-13. Hydrogen bonding and ionic interactions of (A) a pyrimidine dicarboxamide scaffold inhibitor and (B) quinazoline-2-carboxamide scaffold inhibitor (**5b**) within the S_1' and S_1'' pockets are indicated by dashed lines. (C) Overlay of FMBP and **5b** binding modes to MMP-13. Adapted from MMP-13 – inhibitor complexes (PDB: 1XUD and 3WV1).

Here, we describe the development and evaluation of carbon-11 and fluorine-18 labeled MMP-13 selective PET radiotracers based on a quinazoline-2-carboxamide scaffold. To expand upon the structure-activity relationships of this inhibitor class, 10 novel compounds were generated by divergent synthesis with a particular focus on structural modifications that would enable late-

stage radiolabeling. An enzyme inhibition assay was employed to assess inhibitor potency and selectivity against related MMPs. Based on *in vitro* findings, three candidates including the original lead compound **5b**, were selected for radiolabeling and *in vivo* assessment in atherosclerotic *ApoE*$^{-/-}$ mice. Radiotracer pharmacokinetics were characterized by dynamic PET imaging, biodistribution, and plasma radio-metabolite analysis, while atherosclerotic plaque uptake was quantified by *ex vivo* autoradiography. The specificity of the radiotracer demonstrating the best *in vivo* performance was further assessed by homologous and heterologous pre-treatment experiments.

RESULTS AND DISCUSSION

Synthesis of Quinazoline-2-carboxamide Inhibitors

The central quinazolinone scaffold **3** was obtained as previously outlined with minor modifications (Scheme 1).[32] Initially, *tert*-butyloxycarbonyl (Boc) protection of 3,4-difluoroaniline afforded compound **1** (84%). In the presence of 2 equivalents of *n*-butyllithium, ethyl chloroformate was selectively added at the 2-position to generate intermediate **2**, upon removal of the Boc group (64% over two steps). Under acidic conditions, a cyclization with ethyl cyanoformate formed the quinazoline scaffold **3** (73%), which represents a common intermediate with reactive handles for further conjugation.

Scheme 1. Synthesis of Ethyl 5,6-Difluoro-4-oxo-3,4-dihydroquinazoline-2-carboxylate (3)

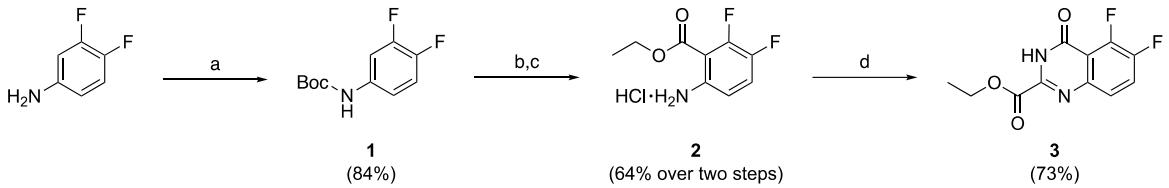

Reagents and conditions: (a) Boc_2O, THF, 60 °C, 16 h (b) *n*-BuLi, THF, -78 °C, 1 h, $ClCO_2Et$, THF, -78–0 °C, 1 h (c) 4 N HCl in dioxane, EtOAc, rt, 4 h (d) $NCCO_2Et$, 1 N HCl in AcOH, 80 °C, 3 h

To investigate the functional group tolerance of the S_1' binding moiety, ethyl ester aminolysis of **3** was performed with several benzylamines to produce the amide intermediates **4a-d** (46-51%, Scheme 2). Higher benzylamine loadings improved conversion but also promoted nucleophilic aromatic substitution at the 5-position and by-products that were difficult to separate by chromatography. The 3-hydroxy- and 3-methoxy-substituted derivatives **4a** and **4b** represent intermediates toward the synthesis of phenolic precursor (**5a**) for subsequent radiolabeling with [^{11}C]iodomethane ([^{11}C]CH_3I) to obtain [^{11}C]**5b** and the corresponding standard compound (**5b**), respectively. The 4-methoxybenzyl and 4-fluoro-3-methylbenzyl intermediates **4c** and **4d** were synthesized on the basis of modifications that were well-tolerated for the pyrimidine-dicarboxamide inhibitor class.[25]

Scheme 2. Synthesis of Intermediates (4a-d) and 5-Substituted Derivatives (5a-k)

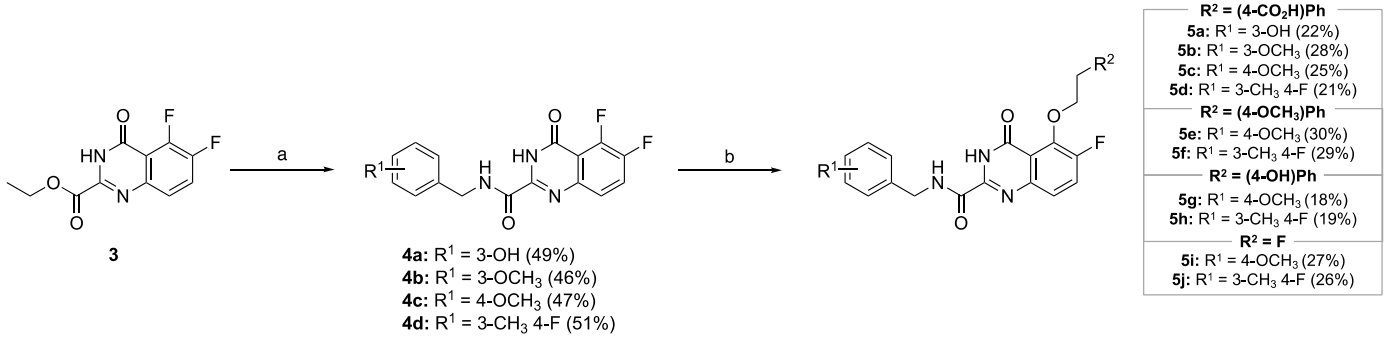

Reagents and conditions: (a) benzylamine, EtOH, 80 °C, 15 h; (b) alcohol, NaH, DMA, 80 °C, 1 h

To further explore the structure-activity relationships of the S_1'' binding moiety, a divergent approach was employed based on nucleophilic aromatic substitution (S_NAr) at the quinazoline 5-fluoro position by various ethyl alcohols (18-30%, Scheme 2). Coupling of 4-(2-hydroxyethyl)benzoic acid afforded the carboxylic acid containing derivatives **5a-d**, which includes the original lead compound **5b** and the radiolabeling precursor **5a**. Replacement of the carboxylic acid with methoxy or hydroxyl groups was envisioned to circumvent potential liability for the organic anion transporter (OAT) and simultaneously represents a convenient strategy for radiolabeling with [^{11}C]CH_3I. Likewise, fluoroethyl derivatives **5i** and **5j** were proposed as alternatives amenable to radiofluorination of the corresponding tosylate precursors.

***In vitro* MMP Inhibition Assays**

To establish inhibitor potency, the half-maximal inhibitory concentrations (IC_{50}) of all intermediates and 5-substituted derivatives were measured against activated MMP-13 (Table 1). Carboxamides **4** exhibit IC_{50} values in the 100 nM range, with the exception of 4-methoxy intermediate **4c**, which was ~3-fold less potent. In line with previous literature, substitutions at the

3-position are well tolerated with a preference toward smaller substituents at the 4-position, as demonstrated for the most potent 4-fluoro-3-methylbenzyl intermediate **4d**.[39] These trends persisted across the remaining derivatives with diminished potency among all compounds containing 4-methoxybenzylamine (**5c**, **5e**, **5g**, **5i**) and a marked improvement for compounds containing 4-fluoro-3-methylbenzylamine (**5d**, **5f**, **5h**, **5j**). Regarding the 5-substituted derivatives, the carboxylic acid containing compounds **5a**, **5b**, and **5d** were most potent and approached the lower limit of detection of the enzyme assay. Under the specified assay conditions, compound **5b** gave an IC_{50} of 1.3 ± 0.2 nM, which represents a ~100-fold increase in potency over the corresponding unsubstituted intermediate **4b** and highlights the contribution of the carboxylate-Lys140 ionic interaction within the S_1'' pocket. Although replacement of the carboxylic acid with methoxy or hydroxyl groups decreased potency, inhibitors **5f** and **5h** were nonetheless still potent, displaying IC_{50} values of 24 ± 1 nM and 12 ± 1 nM, respectively. Furthermore, removal of the arene as demonstrated for the fluoroalkyl derivative **5j** resulted in an IC_{50} of 16 ± 3 nM, comparable to that of the non-carboxylic acid containing derivatives. Taken together, these findings suggest that potent inhibition of MMP-13 can be achieved with quinazoline-2-carboxamides possessing an ethyl ether linkage at the 5-position, irrespective of the presence of an arene. Still, phenethyl derivatives that incorporate a strong hydrogen bond acceptor at the 4-position with sufficient size to deeply occupy the bottom of the S_1'' pocket and exploit the Lys140 interaction are optimal.

Table 1. MMP-13 Inhibitory Activity

Compound	R^1	R^2	MMP-13 IC_{50} (nM)[a]
4a	3-OH	-	149 ± 6
4b	3-OCH_3		118 ± 10
4c	4-OCH_3		313 ± 5
4d	3-CH_3 4-F		106 ± 8
5a	3-OH	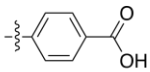	1.3 ± 0.1
5b	3-OCH_3		1.3 ± 0.2
5c	4-OCH_3		2.9 ± 0.5
5d	3-CH_3 4-F		1.2 ± 0.1
5e	4-OCH_3	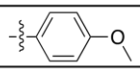	113 ± 5
5f	3-CH_3 4-F		24 ± 1
5g	4-OCH_3	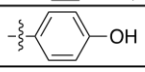	48 ± 7
5h	3-CH_3 4-F		12 ± 1
5i	4-OCH_3	F	127 ± 11
5j	3-CH_3 4-F		16 ± 3
FMBP		-	52 ± 5
Marimastat			2.0 ± 0.2

[a] Measured as the mean ± SEM from a single experiment performed in triplicate.

Using the pyrimidine-dicarboxamide based inhibitor FMBP as a benchmark (MMP-13 IC_{50}: 52 ± 5 nM), the selectivity profiles among inhibitors with greater MMP-13 potency were evaluated against MMP-1, -2, -8, -9, and -10 (Table 2). Remarkably, no appreciable inhibition of MMP-1, -2 or -9 was detected below 10 μM. Consistent with previous reports, collagenase MMP-8 and stromelysin MMP-10 represent the primary off-targets for this inhibitor class.[32] Among inhibitors with identical substituents at the 5-position, a significant decrease in MMP-13 selectivity was observed for derivatives containing 4-methoxybenzylamine (*i.e.*, **5c** and **5g**). Regarding modifications at the 5-position, the carboxylic acid and hydroxyl containing derivatives **5a-d** and **5h** displayed greater selectivity with respect to MMP-8 (IC_{50}: ≥1400 ± 200 nM), in comparison to the methoxyphenyl or fluoroalkyl derivatives **5f** and **5j** (IC_{50}: 780 ± 80 nM and 1200 ± 100 nM). While each of the synthesized compounds were highly selective against MMP-10 (IC_{50}: ≥2500 ±

300 nM), methoxyphenyl and hydroxyl containing derivatives **5f-h** (IC_{50}: ≥6800 ± 1000 nM) were least potent towards this off-target.

Table 2. MMP Selectivity Profiles

	IC_{50} (nM)[a]					
Compound	MMP-1	MMP-2	MMP-8	MMP-9	MMP-10	MMP-13 Fold Selectivity[c]
5a	>10^4	>10^4	2100 ± 160	>10^4	2800 ± 200	1600 ± 175
5b	>10^4	>10^4	2400 ± 130	>10^4	3200 ± 240	1800 ± 300
5c	>10^4	>10^4	1400 ± 140	>10^4	2700 ± 320	483 ± 96
5d	>10^4	>10^4	1700 ± 190	>10^4	2500 ± 220	1400 ± 200
5f	>10^4	>10^4	780 ± 80	>10^4	9100 ± 920	33 ± 3.4
5g	>10^4	>10^4	1500 ± 100	>10^4	6800 ± 980	32 ± 4.8
5h	>10^4	>10^4	2200 ± 240	>10^4	6900 ± 760	183 ± 25
5j	>10^4	>10^4	1200 ± 70	>10^4	3100 ± 400	75 ± 15
FMBP[b]	>10^4	>10^5	>10^5	>10^5	>10^4	>1900
Marimastat	1.0 ± 0.04	5.6 ± 0.2	1.3 ± 0.1	4.7 ± 0.2	69 ± 2.5	-

[a]Measured as the mean ± SEM from a single experiment performed in triplicate.

[b]FMBP IC_{50} values for MMP-2, -8, -9 obtained from the literature under similar assay conditions.[30]

[c]Fold selectivity calculated as a ratio of the MMP-13 IC_{50} / MMP-8 IC_{50} ± SEM.

In line with previous reports, the carboxylic acid containing inhibitor **5b** represented the most promising candidate of the quinazoline-2-carboxamide inhibitor class, with significantly greater potency and comparable MMP-13 selectivity to FMBP (1900 vs 1800 ± 300-fold).[32] However, as a potential substrate of the OAT, as discovered for several carboxylate-containing MMP-13 inhibitors[39,42], non-carboxylic acid derivatives were additionally synthesized. Moreover, in pursuit of optimizing radiotracer pharmacokinetics for vascular imaging, we hypothesized that evaluating structural diversity and varying lipophilicities would be informative. The remaining compounds retained adequate MMP-13 selectivity (32 ± 5 to 183 ± 25-fold) while simultaneously providing a robust strategy for radiolabeling with carbon-11 or fluorine-18. Taking these factors

into consideration, compounds **5b**, **5f**, and **5j** were selected as candidates for radiolabeling and subsequent biological evaluations.

Synthesis of Fluorine-18 Radiolabeling Precursors (9 and 10)

We proposed to radiolabel **5j** by ^{18}F-fluorination of the corresponding tosylate precursor (Scheme 3). Initially, mono-tetrahydropyranyl (THP) protection of ethylene glycol was performed to afford 2-[(tetrahydro-2*H*-pyran-2-yl)oxy]ethan-1-ol (compound **6,** 79%).[43] The THP protecting group was selected for its stability under strongly basic conditions, as in the following S_NAr reaction, mediated by sodium hydride. Coupling of **6** to intermediate **4d** was conducted under identical conditions used for the formation of the 5-substituted derivatives **5a-j** to obtain compound **7** (75%). THP ether hydrolysis was achieved under mild conditions employing catalytic *para*-toluenesulfonic acid in methanol to yield compound **8** (75%). Tosylation of the resulting free alcohol was completed by activation of tosyl chloride with pyridine to give precursor **9** (84%). A DMF-aminal protection strategy was further employed to form an imidazolidine ring under Vilsmeier conditions and provide precursor **10** (85%).[32]

Scheme 3. Synthesis of the Fluorine-18 Radiolabeling Precursors (9 and 10)

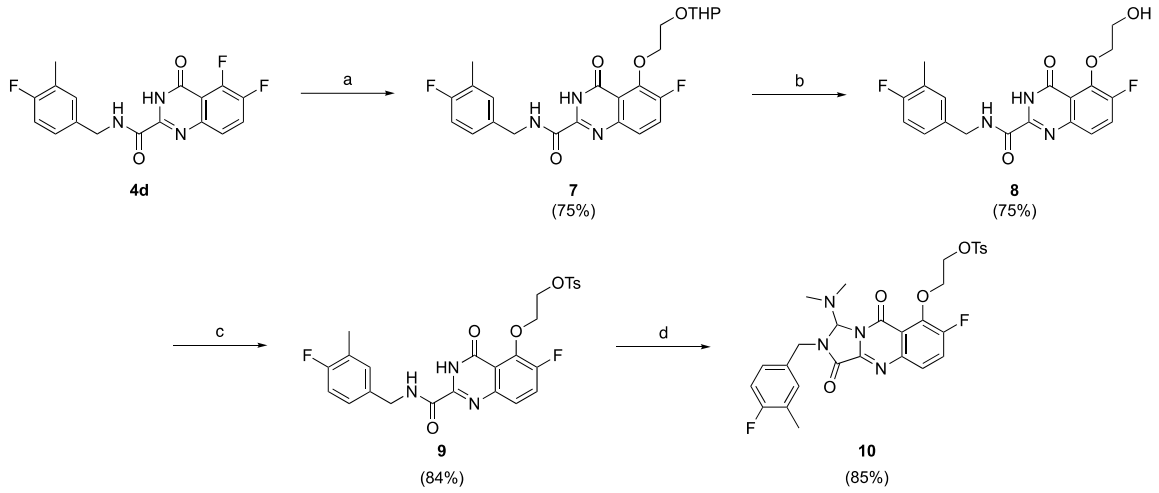

Reagents and conditions: (a) $HO(CH_2)_2OTHP$ (**6**), NaH, DMA, 80 °C, 1 h (b) TsOH, MeOH, rt, 1 h (c) TsCl, pyridine, 0 °C, 4 h (d) $(COCl)_2$, DMF, THF, 0 °C to rt, 2 h.

Radiolabeling Optimization

Radiolabeling of **5b** and **5f** was proposed by ^{11}C-methylation of the corresponding phenolic precursors **5a** and **5h** with [^{11}C]CH_3I (Table 3). Regioselective ^{11}C-methylation was achieved using predicted pK_a values and adjusting the equivalents of tetrabutylammonium hydroxide (TBAOH) required to deprotonate the desired phenol. For precursor **5a**, addition of 3 equivalents of TBAOH was expected to yield **[^{11}C]5b** in the presence of the unprotected carboxylic acid and pyrimidine ring system (Entry 1). Indeed, fewer equivalents of TBAOH was detrimental to selectivity (Entry 2) and additional equivalents did not appreciably improve radiochemical conversion (RCC, Entries 3 and 4). Maintaining this quantity of base, 80 °C afforded the highest conversion, with lower temperatures slowing reaction rates (Entry 5) and higher temperatures likely having deleterious effects on precursor stability (Entry 6). Prolonging the reaction time from 2 to 3 min led to a marginal improvement and optimally afforded **[^{11}C]5b** in 64% RCC (Entry 7).

Applying the same approach for precursor **5h**, which lacks the carboxylic acid, 2 equivalents of TBAOH was predicted to deprotonate the desired phenol. Under the optimal conditions identified for the formation of **[^{11}C]5b** with 1 fewer equivalent of base, **[^{11}C]5f** was obtained in 69% RCC (Entry 1). Additional TBAOH led to selective formation of an unidentified side product (Entry 2). Radiochemical identities of **[^{11}C]5b** and **[^{11}C]5f** were confirmed using radio-HPLC by co-injection of unlabelled **5b** and **5f**, respectively (Figures S5 & S6).

Table 3. [^{11}C]5b and [^{11}C]5f Methylation Optimization

Entry	Prec.[a]	TBAOH (equiv.)	Temp. (°C)	Time (min)	RCC (%)
1	**5a**	3	80	2	59
2		2	80	2	10
3		3.5	80	2	61
4		4	80	2	61
5		3	60	2	35
6		3	100	2	32
7		3	80	3	64
1	**5h**	2	80	3	69
2		3			0

[a]10 mM precursor, 106 µL DMSO, dc. RCC determined by radio-HPLC (n = 1).

As previously indicated, formation of **[^{18}F]5j** was proposed by radiofluorination of the corresponding tosylate precursor **9** (Table 4). Initial attempts using K_2CO_3 and Kryptofix® (K_{222}) at varying concentrations were unsuccessful due to base-mediated precursor decomposition (Entry 1). To this end, weak bases such as tetrabutylammonium mesylate (Bu_4NOMs) and tetrabutylammonium triflate (Bu_4NOTf) were employed as recommended for base-sensitive scaffolds[44], but only afforded trace amounts of product (Entries 2 and 3). Attempts at radiofluorination of precursor **9** with the fewer equivalents of a moderately weak base such as tetraethylammonium bicarbonate (TEAB) proved to be more effective but yields remained

insufficient (Entry 4). As an alternative strategy, precursor **10** was synthesized with a DMF-aminal protecting group to reduce base-sensitivity and improve reactivity towards [^{18}F]fluoride. Using 2 equivalents of TEAB, the DMF-protected **[^{18}F]5j** intermediate was optimally formed within 10 min in 59% RCC and slow progression thereafter (Entry 5). Lesser or greater quantities of TEAB had deleterious effects on RCC (Entries 6 and 7). Higher reaction temperatures caused product decomposition at prolonged reaction times (Entry 8). Quantitative deprotection was achieved with 6 M HCl at 100 °C for 10 min, as determined by the disappearance of the DMF-protected radio-fluorinated intermediate and formation of **[^{18}F]5j**, confirmed by co-injection of unlabelled **5j** using radio-HPLC (Figure S7).

Table 4. [^{18}F]5j Fluorination Optimization

Entry	Prec.[a]	Base	Base equiv.	Temp. (°C)	RCC (%) 10 min	RCC (%) 20 min
1	**9**	K_2CO_3/K_{222}[b]	4 or 8	100	0	0
2		Bu_4NOMs	4 or 8	100	<1	<1
3		Bu_4NOTf	4 or 8	100	<1	<1
4		TEAB	2 or 4	100	2	2
5	**10**	TEAB	2	100	59	61
6			1	100	43	45
7			4	100	51	53
8			2	120	56	46

[a]13.5 mM precursor, 250 μL DMSO, RCC determined by radio-TLC (n = 1)

[b] 1:2.2 molar ratio of K_2CO_3:K_{222}

Radiotracer Automation, Formulation Stability and Lipophilicity

Automated radiosyntheses were developed for **[^{11}C]5b** and **[^{11}C]5f** using a Synthra MeIPlus Research module, while a two-step production of **[^{18}F]5j** was performed using the GE TRACERlab FX2 N (Figure 2). Radiotracers were labelled under the optimized conditions, purified with in-line semi-preparative HPLC, and reformulated in 10% EtOH/saline suitable for *in*

vivo evaluation. **[^{11}C]5b** was obtained in radiochemical yields of 32 ± 2% (from [^{11}C]CH_3I) within 48 ± 2 min, >99% radiochemical purity, and a molar activity of 11 ± 2 GBq·µmol^{-1} at the end of synthesis (EoS) (n = 5). **[^{11}C]5f** was obtained in radiochemical yields of 35 ± 5 % (from [^{11}C]CH_3I) within 55 ± 10 min, >99% radiochemical purity, and a molar activity of 12 ± 3 GBq·µmol^{-1} at EoS (n = 6). **[^{18}F]5j** was obtained in radiochemical yields of 44 ± 3% within 92 ± 8 min, >99% radiochemical purity, and a molar activity of 53 ± 5 GBq·µmol^{-1} at EoS (n = 8). Radiotracer stability in formulation was assessed up to 75 min with no observable degradation during this period (Figure S9).

Radiotracer lipophilicity was assessed by determination of the octanol-PBS distribution coefficient (log*D*, n = 2). Due to the anionic nature of the carboxylate at physiological pH, **[^{11}C]5b** was least lipophilic (1.16 ± 0.03), while sequential increases were observed for **[^{18}F]5j** (3.09 ± 0.03) and **[^{11}C]5f** (3.76 ± 0.32) upon removal and replacement of the terminal arene, respectively.

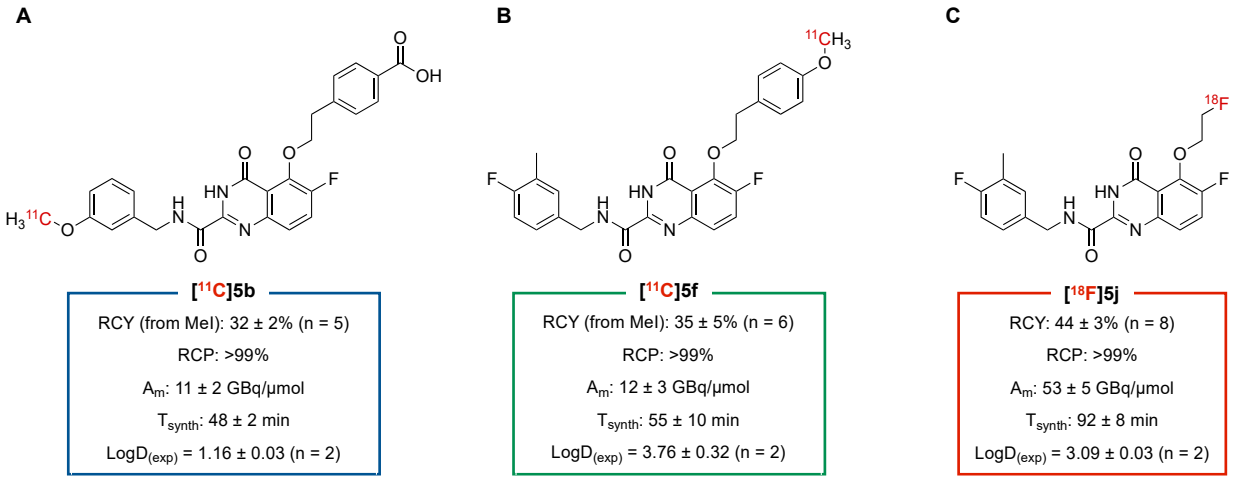

Figure 2. Chemical structures and automated radiosyntheses of (A) **[^{11}C]5b**, (B) **[^{11}C]5f**, (C) **[^{18}F]5j**.

Dynamic PET imaging and Radiotracer Kinetics

With the target radiotracers in hand, dynamic PET imaging was conducted over 60 minutes to establish *in vivo* pharmacokinetics in atherosclerotic *ApoE*$^{-/-}$ mice (Figure 3). Following intravenous administration, **[^{11}C]5b**, **[^{11}C]5f**, **[^{18}F]5j** cleared from the blood pool (t_{max} = 0.625 min) with prolonged washout after 30 minutes (Fig. 3B). Myocardial retention fell below 0.5 %ID·cc^{-1} for all 3 candidates and was greatly reduced relative to the first generation MMP-13 selective radiotracer [^{18}F]FMBP (~5 %ID·cc^{-1}). Low cardiac activity is an important property for reducing spillover and permitting quantification of the surrounding vasculature (Figures 3A & 3C). Uniquely, **[^{11}C]5b** immediately accumulated in the liver with peak uptake reaching 25.29 ± 2.04 %ID·cc^{-1} (Figures 3A & 3D). Accelerated washout from the liver was subsequently observed with concomitant increase in intestinal uptake over the course of the scan, in accordance with a hepatobiliary excretion route (Figure 3A). In contrast to **[^{11}C]5b** and [^{18}F]FMBP, which is retained in the liver (~12 %ID·cc^{-1}), peak liver uptake of **[^{11}C]5f** and **[^{18}F]5j** reached 9.30 ± 1.33 %ID·cc^{-1} and 6.43 ± 0.08 %ID·cc^{-1}, respectively, with continual washout thereafter (Figures 3A & 3D). This marked decrease greatly reduces radioactivity in the thoracic cavity to facilitate vascular imaging and addresses a key limitation of MMP-13 targeted radiotracers based on a pyrimidine-dicarboxamide scaffold (Figure 3A).[30] Notably, peak kidney uptake of **[^{11}C]5b** reached 21.01 ± 1.48 %ID·cc^{-1} and was largely sustained without clearance into the bladder (Figures 3A & 3E). This suggests the possibility for OAT-mediated accumulation, as previously demonstrated for several carboxylic acid-containing MMP-13 selective inhibitors[39], and is consistent with the predominant expression of this transporter in renal proximal tubule cells.[42] Accordingly, the non-carboxylic acid derivatives **[^{11}C]5f** and **[^{18}F]5j** displayed distinct kinetics with peak kidney uptake reaching 7.40 ± 0.48 %ID·cc^{-1} and 4.42 ± 0.44 %ID·cc^{-1}, respectively, with substantial clearance

over time (Figure 3E). Moreover, **[^{18}F]5j** preferentially exhibited renal clearance as demonstrated by urinary excretion (Figure 3A).

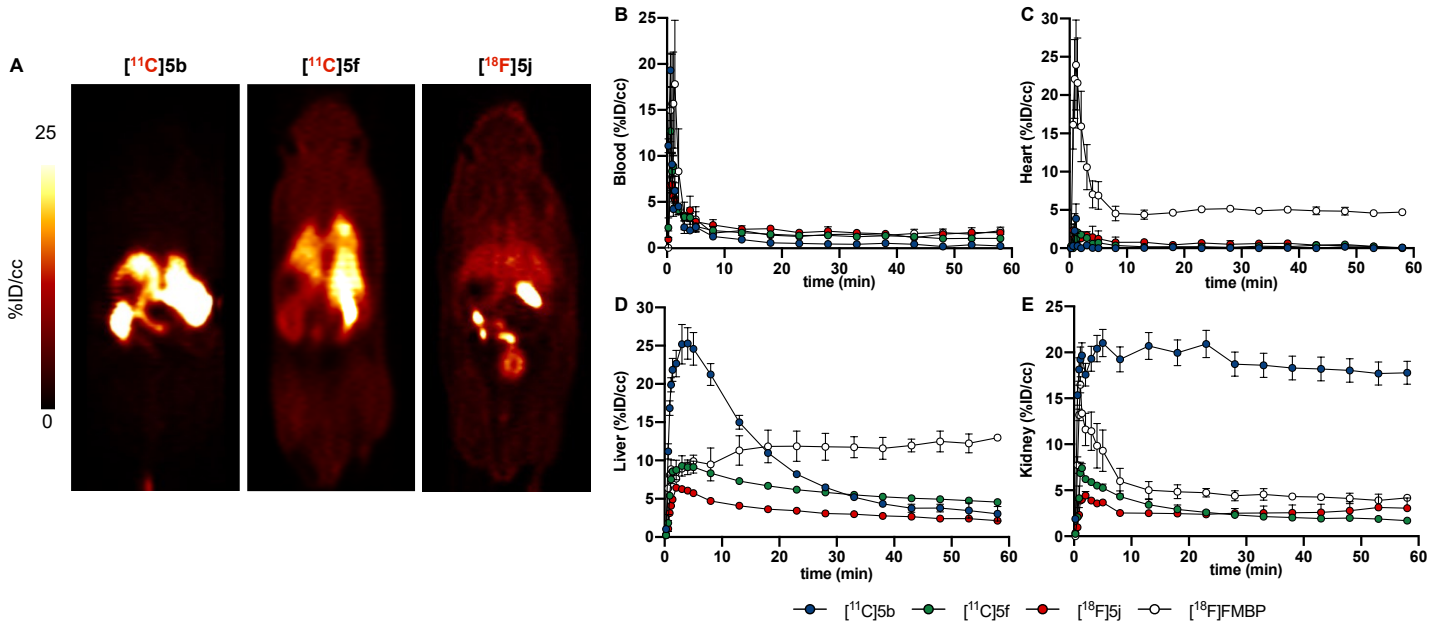

Figure 3. Radiotracer distribution in *ApoE*$^{-/-}$ mice. (A) Representative dynamic PET images (summed 0-60 minutes, coronal axis). (B-E) Comparative time-activity curves for the blood, heart, liver, and kidney (n = 2 per group).

Biodistribution and Plasma Metabolism

The biodistribution of each radiotracer was assessed by dissection at 30-minutes post-injection in *ApoE*$^{-/-}$ mice (Figure 4A). Consistent with *in vivo* findings, **[^{11}C]5b** rapidly cleared from the blood with 0.49 ± 0.20 %ID·g^{-1} remaining while **[^{11}C]5f** and **[^{18}F]5j** were relatively slower with 1.83 ± 0.19 %ID·g^{-1} and 3.28 ± 0.42 %ID·g^{-1}, respectively, at this timepoint (*P < 0.03). In a separate time-course experiment, **[^{18}F]5j** blood radioactivity continued to decrease between 30 and 60 minutes and stabilized thereafter (Figure S11). Minimal accumulation of

myocardial activity was observed across all radiotracers with ~1 %ID·g^{-1} remaining. Regarding metabolic and excretory organs, **[^{11}C]5b** liver uptake was moderate at 7.29 ± 0.73 %ID·g^{-1} with predominant accumulation in the kidney and intestine at 30.95 ± 4.64 %ID·g^{-1} and 53.05 ± 5.95 %ID·g^{-1}, respectively. In contrast, **[^{11}C]5f** had significantly decreased uptake in the kidney and intestine (<7 %ID·g^{-1}, **** $P < 0.0001$). **[^{18}F]5j** further displayed a significant reduction in liver uptake (3.32 ± 0.41 %ID·g^{-1}, ***$P < 0.0002$). Relatively low levels of radioactivity (~2 %ID·g^{-1}) were observed in all other measured organs except for the pancreas (**[^{11}C]5f**: 3.27 ± 1.12 %ID·g^{-1} and **[^{18}F]5j**: 2.14 ± 0.48 %ID·g^{-1}) and spleen (**[^{11}C]5b**: 2.11 ± 0.69 %ID·g^{-1}).

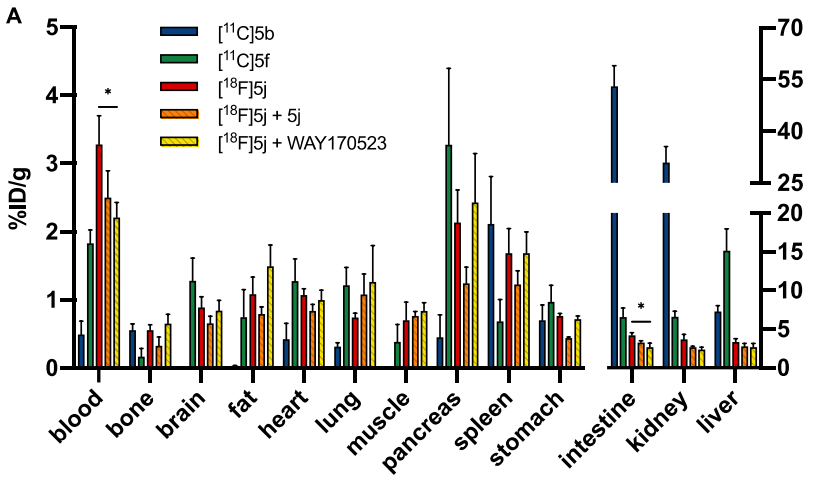

B

Fraction (%)	[^{11}C]5b	[^{11}C]5f	[^{18}F]5j	[^{18}F]5j + 5j	[^{18}F]5j + WAY170523
Parent Radiotracer	86 ± 3	70 ± 4	78 ± 3	78 ± 1	87± 2
Polar Metabolites	6 ± 3	22 ± 3	18 ± 4	21 ± 1	9 ± 1
Non-polar Metabolites	9 ± 1	8 ± 1	4 ± 1	2 ± 1	4 ± 1
Extraction Efficiency	91 ± 1	76 ± 2	92 ± 1	95 ± 1	92 ± 1

Figure 4. Radiotracer distribution and plasma stability in *ApoE*$^{-/-}$ mice. (A) Ex vivo biodistribution and (B) plasma radio-metabolite analysis 30 min after intravenous radiotracer administration. 2-way ANOVA: *$P < 0.039$. n = 4 for all groups except [^{11}C]5f, n = 6.

Considering the favourable distribution of **[^{18}F]5j**, additional blocking studies were conducted by pre-treatment with non-radioactive **5j** (2.5 mg/kg, IV) or WAY170523 (7.5 mg/kg, IV), a potent and selective commercially available MMP-13 inhibitor.[45,46] Only minor differences were measured upon homologous blocking with **5j**, although limited aqueous solubility restricted

the administrable dose. Upon heterologous blocking with WAY170523, blood and intestinal radioactivity were significantly reduced by 33% and 36% (*$P < 0.04$) with no further differences in peripheral organs, reflecting low target expression in these tissues.

In parallel, radiotracer stability in plasma was also assessed at the same timepoint in *ApoE*$^{-/-}$ mice (Figure 4B). Radio-metabolite analysis revealed that all 3 tracers were largely intact with 70–86% of total plasma radioactivity representing the unmetabolized parent fraction after 30 minutes with an apparent dependence on lipophilicity. Remaining radioactivity was mainly attributed to polar radio-metabolites. No differences in **[^{18}F]5j** metabolism were detected under homologous blocking conditions, while a significant increase in the parent fraction was observed under heterologous blocking conditions (**$P = 0.003$). This presumably suggests that homologous blocking did not saturate metabolic enzymes, while WAY170523 inhibited degradation or modification of **[^{18}F]5j**. The measured extraction efficiencies (≥76%) suggest representative sampling of plasma radioactivity.

Aortic Autoradiography and Oil Red O Staining

Considering the challenges associated with accurate non-invasive detection and quantification of aortic plaques in mice, *ex vivo* aortic autoradiography was employed to provide higher resolution images and enable histological colocalization (Figure 5). **[^{11}C]5b** did not accumulate in atherosclerotic plaques indicated by Oil Red O (ORO) positive lipid-rich regions as indicated by homogenous and comparatively low aortic uptake at 52.97 ± 9.83 %ID·m^{-2}. Conceivably, rapid excretion provides insufficient time for radiotracer circulation. Replacement of the carboxylic acid with a methyl ether, as for **[^{11}C]5f**, restored *in vivo* functionality as focal uptake could be detected in ORO positive regions, albeit with moderate uptake at 129.8 ± 42.05 %ID·m^{-2}. While the carboxylic acid has been shown to significantly drive *in vitro* target affinity

and selectivity, this molecule is likely susceptible to OAT transport *in vivo* and is unsuitable as an MMP-13 targeted radiotracer for atherosclerosis. Most favourably, **[^{18}F]5j** displayed the highest overall uptake at 270.0 ± 8.06 %ID·m^{-2} and greatest co-localization to ORO positive regions. To further assess the specificity of the signal, *in vivo* homologous and heterologous blocking was performed. Pre-treatment with non-radioactive **5j**, 15 minutes prior to intravenous radiotracer administration, resulted in a 23% decrease in aortic plaque uptake to 208.2 ± 13.27 %ID·m^{-2}, indicating an extent of saturable binding (*P = 0.047). Gratifyingly, pre-treatment with WAY170523 further reduced aortic plaque uptake by 36% to 173.4 ± 27.38 %ID·m^{-2}, providing evidence of specific binding to MMP-13 (**P = 0.0041).

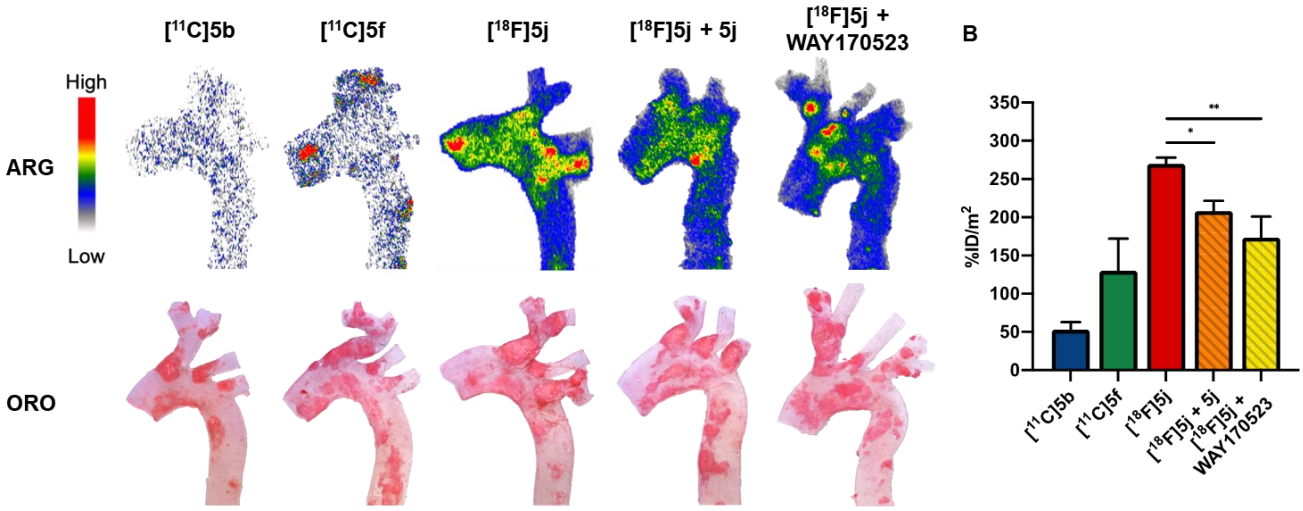

Figure 5. Autoradiography and Oil Red O (ORO) staining of *ApoE*$^{-/-}$ aortae. (A) Representative *ex vivo* aortic autoradiographs 30 min after intravenous radiotracer administration with corresponding ORO staining. (B) Aortic plaque uptake. 1-way ANOVA: **P = 0.0041, *P = 0.047. n = 4 per group except [^{18}F]5j, n = 5.

CONCLUSION

In the current study, we sought to develop and evaluate MMP-13 selective PET radiotracers based on quinazoline-2-carboxamide inhibitors for imaging extracellular matrix remodeling in atherosclerotic plaques. Several novel inhibitors were synthesized to further explore the structure-activity relationships of this class of molecules with an eye towards molecular imaging. *In vitro* enzyme assays revealed that modifications within the S_1'-interacting arene are well tolerated, except for larger groups at the *para*-position. In line with other reports, a substantial increase in potency and selectivity can be achieved by occupying the S_1'' pocket with an ethyl ether linkage conjugated to the quinazoline scaffold at the 5-position. Most notably, phenethyl derivatives bearing a carboxylic acid at the 4-position are potent and selective *in vitro* as they can exploit an additional interaction with Lys140 at the bottom of the S_1'' pocket. However, these molecules can be substrates of the OAT *in vivo*, and alternative inhibitors were synthesized. Despite replacement of the carboxylic acid or removal of the terminal S_1''-interacting arene, these derivatives still retained significant MMP-13 potency and selectivity and facilitated late-stage radiolabeling. Based on these findings, high yielding automated radio-syntheses with carbon-11 and fluorine-18 were established for inhibitors **5b**, **5f,** and **5j** to enable *in vivo* assessments in atherosclerotic *ApoE*$^{-/-}$ mice and characterization of radiotracer pharmacokinetics.

Dynamic PET imaging and *ex vivo* biodistribution revealed that the carboxylic acid containing radiotracer **[^{11}C]5b** exhibited rapid hepatobiliary excretion with retention of radioactivity in the kidney, suggestive of OAT mediated transport. *Ex vivo* aortic autoradiography further revealed that **[^{11}C]5b** does not accumulate in atherosclerotic plaques, rendering it unsuitable as an MMP-13 targeted radiotracer for this application. In contrast, the non-carboxylic acid alternatives **[^{11}C]5f** and **[^{18}F]5j** exhibited vastly improved pharmacokinetic profiles with low

uptake in metabolic organs, and minimal retention of radioactivity in the myocardium, addressing a previous limitation of first generation MMP-13 targeted radiotracers based on a pyrimidine-dicarboxamide scaffold. Most importantly, *in vivo* utility was restored as focal uptake of **[^{11}C]5f** and **[^{18}F]5j** could be detected in atherosclerotic plaques, with **[^{18}F]5j** displaying the highest overall uptake and greatest colocalization to lipid-rich ORO-positive regions. Furthermore, homologous and heterologous MMP-13 blocking studies with **[^{18}F]5j** significantly reduced atherosclerotic plaque uptake, confirming specific target engagement. Overall, we have demonstrated that the quinazoline-2-carboxamide core represents an excellent scaffold for MMP-13 selective PET radiotracer development and identified **[^{18}F]5j** as a promising lead candidate which possesses favourable pharmacokinetics properties for vascular imaging. Future studies will focus on increasing inhibitor selectivity and reducing lipophilicity to improve the extent of specific binding and accelerate blood clearance.

EXPERIMENTAL SECTION

General Information

Chemical reagents and solvents were purchased from commercial sources and used without further purification. All moisture or air sensitive reactions were performed under inert atmosphere in flame dried glassware. Reaction progress was monitored by thin layer chromatography on silica gel-coated plates and visualized directly with UV light (254 and 280 nm) or following staining with a potassium permanganate solution. Products were purified by flash column chromatography using a Biotage Isolera One system. Compound identity was confirmed with a Magritek Spinsolve 80 MHz Spectrometer and characterization was completed by ^{1}H/^{13}C NMR with a Bruker AVANCE III 400 or 600 MHz spectrometer using DMSO-d_6 or $CDCl_3$ as a solvent (reference: 2.54 or 7.26 ppm) and analyzed using Mnova software. High resolution mass spectrometry data

was acquired using a Waters Synapt G1, HRes and Ion Mobility, Time of Flight Mass Spectrometer or a Kratos Concept – Magnetic Sector Electron Impact Mass Spectrometer. All target compounds are >95% pure according to analysis using a Waters Xevo TQD with an Acquity UPLC H-Class Plus system.

Chemical Synthesis

*tert-Butyl N-(3,4-difluorophenyl)carbamate (**1**).* To a solution of 3,4-difluoroaniline (3.00 mL, 30.3 mmol, 1.0 equiv.) in anhydrous THF (30.0 mL) was added di-*tert*-butyl dicarbonate (7.65 mL, 33.3 mmol, 1.1 equiv.). The mixture was refluxed at 60 °C for 16 h. The solution was then cooled to room temperature and concentrated under reduced pressure. The residue was re-suspended in EtOAc and washed with 0.1 M HCl followed by saturated $NaHCO_3$. The organic layer was collected, dried over Na_2SO_4, filtered, and concentrated under reduced pressure. The residue was crystallized from hexanes to obtain the title compound as a white solid (5.85 g, 25.52 mmol, 84%). ^{1}H-NMR (80 MHz, $CDCl_3$): δ 7.57-7.28 (1H, ddd, J = 12.8, 7.2, 3.2 Hz), 7.24-6.78 (2H, m), 6.44 (1H, br), 1.51 (9H, s) ppm. HRMS (EI, m/z): $[M]^+$ calculated $C_{11}H_{13}F_2NO_2$ as 229.0914, found as 229.0899. Spectrum in accordance with literature.[47]

*Ethyl 6-amino-2,3-difluorobenzoate hydrochloride (**2**).* To a solution of **1** (3.89 g, 16.98 mmol, 1.0 equiv.) in anhydrous THF (38.6 mL), was added dropwise *n*-butyl lithium (1.6 M in hexane, 23.4 mL, 37.4 mmol, 2.2 equiv.) at -78 °C. The mixture was stirred at -78 °C for 1 h before a solution of ethyl chloroformate (1.79 mL, 18.72 mmol, 1.1 equiv.) in anhydrous THF (11.7 mL) was added dropwise over 30 min. The reaction was warmed to 0 °C and stirred for an additional 1 h. The reaction was then quenched by dropwise addition of saturated NH_4Cl (40 mL) and extracted with EtOAc. The combined organics were washed with brine, dried over Na_2SO_4, filtered, and concentrated under reduced pressure to obtain yellow oil. The crude product was utilized in the

following reaction without further purification. To a solution of the yellow oil in EtOAc (7.57 mL) was added 4 N HCl in dioxane (30.3 mL). The mixture was stirred at room temperature for 4 h before diethyl ether was added and the precipitate was collected by filtration to obtain the title compound as a white solid (2.59 g, 10.90 mmol, 64% over 2 steps). ^{1}H-NMR (80 MHz, $(CD_3)_2SO$): δ 8.16 (3H, br), 7.55-7.19 (1H, m), 6.72-6.53 (1H, ddd, J = 8.8, 4.0, 1.6 Hz), , 4.34 (2H, q, J = 7.2 Hz), 1.33 (3H, t, J = 7.2 Hz) ppm. ^{13}C-NMR (150 MHz, $(CD_3)_2SO$): δ 164.8, 149.2 (dd, J = 254, 14 Hz) 146.6, 141.2 (dd, J = 234, 14 Hz) 122.0 (dd, J = 19, 2 Hz), 118.6 (d, J = 19 Hz), 112.1, 60.9, 14.1 ppm. HRMS (EI, m/z): $[M]^+$ calculated $C_9H_9F_2NO_2$ as 201.0601, found as 201.0610.

*Ethyl 5,6-difluoro-4-oxo-3,4-dihydroquinazoline-2-carboxylate (**3**).* To a solution of **2** (2.59 g, 10.90 mmol, 1.0 equiv.) in 1 N HCl in acetic acid (52.0 mL) was added ethyl cyanoformate (1.18 mL, 11.94 mmol, 1.1 equiv.). The mixture was stirred at 80 °C for 3 h before removal of the solvent under reduced pressure. The residue was re-suspended in EtOH and the precipitate was collected by filtration. The solid was further washed with EtOH to obtain the title compound as a white solid (2.03 g, 7.99 mmol, 73%). ^{1}H-NMR (400 MHz, $(CD_3)_2SO$): δ 12.78 (1H, br), 8.05-7.98 (1H, m), 7.76-7.72 (1H, m), 4.42 (2H, q, J = 7.0 Hz), 1.38 (3H, t, J = 7.0 Hz) ppm. ^{13}C-NMR (600 MHz, $(CD_3)_2SO$): δ 159.8, 158.3, 148.4 (dd, J = 12.0, 246 Hz), 147.5 (dd, J = 15, 264 Hz), 144.8 (d, J = 1.5 Hz), 143.8 (d, J = 1.5 Hz), 125.2 (dd, J = 6.0, 7.5 Hz), 123.8 (d, J = 20 Hz), 113.9 (d, J = 3.0 Hz), 62.8, 13.9 ppm. HRMS (EI, m/z): $[M]^+$ calculated $C_{11}H_8F_2N_2O_3$ as 254.0503, found as 254.0522.

*5,6-Difluoro-N-[(3-hydroxyphenyl)methyl]-4-oxo-3,4-dihydroquinazoline-2-carboxamide (**4a**).* To a solution of **3** (363 mg, 1.43 mmol, 1.0 equiv.) in anhydrous EtOH (7.15 mL) was added 3-hydroxybenzylamine (264 mg, 2.15 mmol, 1.5 equiv.). The reaction mixture stirred at 80 °C for 15 h before removal of the solvent under reduced pressure. The residue was re-suspended in EtOAc

and extracted with 0.1 M HCl. The combined organics were washed with brine, dried over Na_2SO_4, filtered, and concentrated under reduced pressure. The crude mixture was purified by column chromatography (10-50% EtOAc/hexane) to obtain the title compound as a white solid (232 mg, 0.70 mmol, 49%). ^{1}H-NMR (600 MHz, $(CD_3)_2SO$): δ 12.46 (1H, br), 9.51 (1H, t, J = 6.4 Hz), 9.36 (1H, s), 7.98-7.94 (1H, m), 7.63-7.60 (1H, m), 7.11-7.09 (1H, m), 6.76-6.74 (2H, m), 6.64-6.63 (1H, m), 4.38 (2H, d, J = 6.4 Hz) ppm. ^{13}C-NMR (150 MHz, $(CD_3)_2SO$): δ 159.1, 158.2, 157.4, 148.0 (dd, J = 11, 245 Hz), 147.6 (dd, J = 14, 263 Hz), 146.1, 144.7, 140.1, 129.3, 124.3, 123.6 (d, J = 19 Hz), 118.1, 114.3, 113.9, 113.6, 42.6 ppm. HRMS (EI, m/z): $[M]^+$ calculated $C_{16}H_{11}F_2N_3O_3$ as 331.0768, found as 331.0760.

*5,6-Difluoro-N-[(3-methoxyphenyl)methyl]-4-oxo-3,4-dihydroquinazoline-2-carboxamide **(4b)**.* Following the procedure described for **4a**, compound **4b** was prepared from compound **3** and 3-methoxybenzylamine. The crude mixture was purified by column chromatography (10-40% EtOAc/hexane) to obtain the title compound as a white solid (314 mg, 0.91 mmol, 46%). ^{1}H NMR (600 MHz, $(CD_3)_2SO$): δ 9.26 (1H, t, J = 6.0 Hz), 7.62 - 7.59 (1H, m), 7.53 – 7.50 (1H, m), 7.28 – 7.25 (1H, m), 6.94 – 6.92 (2H, m), 6.85 – 6.83 (1H, m), 4.47 (2H, d, 6.0 Hz), 3.77 (3H, s) ppm. ^{13}C-NMR (150 MHz, $(CD_3)_2SO$): δ 168.8, 165.6, 159.3, 156.7, 149.4, 146.9 (dd, J = 14, 243 Hz), 145.3 (dd, J = 14, 240 Hz), 141.1, 129.3, 123.0 (dd, J = 3.0, 6.0 Hz), 119.9 (d, J = 18 Hz), 119.5, 113.4 (d, J = 3.0 Hz), 113.1, 112.1, 55.0, 42.5 ppm. HRMS (EI, m/z): $[M]^+$ calculated $C_{17}H_{13}F_2N_3O_3$ as 345.0925, found as 345.0916.

*5,6-Difluoro-N-[(4-methoxyphenyl)methyl]-4-oxo-3,4-dihydroquinazoline-2-carboxamide **(4c)**.* Following the procedure described for **4a**, compound **4c** was prepared from compound **3** and 4-methoxybenzylamine. The crude mixture was purified by column chromatography (10-40% EtOAc/hexane) to obtain the title compound as a white solid (563 mg, 1.63 mmol, 47%). ^{1}H-NMR

(600 MHz, $(CD_3)_2SO$): δ 12.43 (1H, br), 9.49 (1H t, J = 6.1 Hz), 7.98-7.93 (1H, m), 7.62-7.59 (1H, m), 7.28-7.26 (2H, m), 6.90-6.87 (2H, m), 4.39 (2H, d, J = 6.4 Hz), 3.72 (3H, s) ppm. ^{13}C-NMR (150 MHz, $(CD_3)_2SO$): δ 159.1, 158.4, 158.2, 147.9 (dd, J = 11, 245 Hz), 147.6 (dd, J = 14, 263 Hz), 146.2, 144.7, 130.7, 129.0, 124.3, 123.6 (d, J = 19 Hz), 113.7, 113.6, 55.1, 42.2 ppm. HRMS (EI, m/z): $[M]^+$ calculated $C_{17}H_{13}F_2N_3O_3$ as 345.0925, found as 345.0917.

*5,6-Difluoro-N-[(4-fluoro-3-methylphenyl)methyl]-4-oxo-3,4-dihydroquinazoline-2-carboxamide (**4d**).* Following the procedure for described **4a**, compound **4d** was prepared from compound **3** and 4-fluoro-3-methylbenzylamine. The crude mixture was purified by column chromatography (10-40% EtOAc/hexane) to obtain the title compound as a white solid (524 mg, 1.51 mmol, 51%). ^{1}H-NMR (600 MHz, $(CD_3)_2SO$): δ 12.48 (1H, s), 9.59 (1H, t, J = 6.2 Hz), 8.02-7.97 (1H, m), 7.66-7.64 (1H, m), 7.30-7.28 (1H, m), 7.24-7.21 (1H, m), 7.14-7.10 (1H, m), 4.45 (2H, d, J = 6.4 Hz), 2.25 (3H, d, J = 1.7 Hz) ppm. ^{13}C-NMR (150 MHz, $(CD_3)_2SO$): δ 159.8 (d, J = 241 Hz), 159.2, 158.2, 148.0 (dd, J = 11, 245 Hz), 147.7 (dd, J = 14, 263Hz), 146.1, 144.7, 134.6 (d, J = 3.4 Hz), 130.8 (d, J = 5.1 Hz), 126.9 (d, J = 8.1 Hz), 124.3, 123.9 (d, J = 17 Hz), 123.6 (d, J = 19 Hz), 114.7 (d, J = 22 Hz), 113.6, 42.1, 14.2 (d, J = 3.3 Hz) ppm. HRMS (EI, m/z): $[M]^+$ calculated $C_{17}H_{12}F_3N_3O_2$ as 347.0882, found as 347.0876.

*4-{2-[(6-Fluoro-2-{[(3-hydroxyphenyl)methyl]carbamoyl}-4-oxo-3,4-dihydroquinazolin-5-yl)oxy]ethyl}benzoic acid (**5a**).* To a solution of 4-(2-hydroxyethyl)benzoic acid (137 mg, 0.83 mmol, 1.5 equiv.) in anhydrous DMA (5.53 mL) was added sodium hydride (60% oil dispersion, 164 mg, 4.09 mmol, 7.5 equiv), and the mixture was stirred at room temperature for 30 min. Compound **4a** (181 mg, 0.55 mmol, 1.0 equiv.) was added and the mixture was stirred at 80 °C for 1 h. The reaction was cooled to room temperature, acidified with 0.1 M HCl to pH 3−4 and extracted with EtOAc. The combined organics were washed with brine, dried over Na_2SO_4,

filtered, and concentrated under reduced pressure. The crude mixture was purified by preparative TLC (10% MeOH/DCM + 1% formic acid) to obtain the title compound as a white solid (58 mg, 0.12 mmol, 22%). ^{1}H-NMR (600 MHz, $(CD_3)_2SO$): δ 12.87 (1H, br), 12.19 (1H, br), 9.50 (1H, t, J = 6.4 Hz), 9.39 (1H, br), 7.92-7.90 (2H, m), 7.84-7.81 (1H, m), 7.58-7.56 (1H, m), 7.51-7.49 (2H, m), 7.16-7.13 (1H,m), 6.80-6.77 (2H, m), 6.68-6.66 (1H, m), 4.43 (2H, d, J = 6.4 Hz), 4.36 (2H, t, J = 6.9 Hz), 3.23 (2H, t, J = 6.9 Hz) ppm. ^{13}C-NMR (150 MHz, $(CD_3)_2SO$): δ 167.3, 159.3, 158.8, 157.4, 153.8 (d, J = 245Hz), 145.3, 145.2, 145.1, 143.6, 140.1, 129.3, 129.1, 129.0, 128.9, 124.3, 123.1 (d, J = 22Hz), 118.2, 118.0, 114.2, 113.9, 75.2, 42.6, 35.7 ppm. HRMS (ESI+, m/z): calculated $[M+Na]^+$ $C_{25}H_{20}FN_3O_6Na$ as 500.1234, found as 500.1222.

*4-{2-[(6-Fluoro-2-{[(3-methoxyphenyl)methyl]carbamoyl}-4-oxo-3,4-dihydroquinazolin-5-yl)oxy]ethyl}benzoic acid (**5b**).* Following the procedure described for **5a**, compound **5b** was prepared from compound **4b** and 4-(2-hydroxyethyl)benzoic acid. The crude reaction mixture was purified by preparative TLC (10% MeOH/DCM + 1% formic acid) to obtain the title compound as a white solid (79 mg, 0.16 mmol, 28%). ^{1}H-NMR (600 MHz, $(CD_3)_2SO$): δ 12.86 (1H br), 12.18 (1H, s), 9.54 (1H, t, J = 6.4 Hz), 7.92-7.90 (2H, m), 7.84-7.81 (1H, m), 7.58-7.56 (1H, m), 7.51-7.49 (2H, m) 7.30-7.27 (1H, m), 6.95-6.94 (2H, m), 6.87-6.85 (1H, m), 4.48 (2H, d, J = 6.4 Hz), 4.35 (2H, t, J = 6.9 Hz), 3.77 (3H, s), 3.22 (2H, t, J = 6.9 Hz) ppm. ^{13}C-NMR (150 MHz, $(CD_3)_2SO$): δ 167.3, 159.4, 159.3, 158.8, 153.8 (d, J = 245Hz), 145.3, 145.2, 145.1, 143.6, 140.3, 129.4, 129.3, 129.2, 128.8, 124.3, 123.1 (d, J = 21 Hz), 119.6, 118.2, 113.3, 112.3, 75.2, 55.0, 42.6, 35.7 ppm. HRMS (ESI+, m/z): calculated $[M+Na]^+$ $C_{26}H_{22}FN_3O_6Na$ as 514.1390, found as 514.1412.

*4-{2-[(6-Fluoro-2-{[(4-methoxyphenyl)methyl]carbamoyl}-4-oxo-3,4-dihydroquinazolin-5-yl)oxy]ethyl}benzoic acid (**5c**).* Following the procedure described for **5a**, compound **5c** was

prepared from compound **4c** and 4-(2-hydroxyethyl)benzoic acid. The crude reaction mixture was purified by preparative TLC (10% MeOH/DCM + 1% formic acid) to obtain the title compound as a white solid (36 mg, 0.073 mmol, 25%). ^{1}H-NMR (600 MHz, $(CD_3)_2SO$): δ 12.83 (1H, br), 12.12 (1H, br), 9.45 (1H, t, J = 6.1 Hz), 7.87-7.86 (2H, m), 7.79-7.76 (1H, m), 7.53-7.51 (1H, m), 7.46-7.45 (2H, m), 7.28-7.25 (2H, m), 6.90-6.87 (2H, m), 4.39 (2H, d, J = 6.4 Hz), 4.31 (2H, t, J = 6.9 Hz), 3.72 (3H, s), 3.17 (2H, t, J = 6.9 Hz) ppm. ^{13}C-NMR (150 MHz, $(CD_3)_2SO$): δ 167.3, 159.2, 158.8, 158.4, 153.8 (d, J = 244 Hz), 145.3, 145.2, 145.1, 143.6, 130.7, 129.3, 129.2, 129.0, 128.8, 124.2 (d, J = 6.8 Hz), 123.1 (d, J = 22 Hz), 118.2, 113.7, 75.2, 55.1, 42.1, 35.7 ppm. HRMS (ESI+, m/z): calculated $[M+Na]^+$ $C_{26}H_{22}FN_3O_6Na$ as 514.1390, found as 514.1387.

*4-{2-[(6-Fluoro-2-{[(4-fluoro-3-methylphenyl)methyl]carbamoyl}-4-oxo-3,4-dihydroquinazolin-5-yl)oxy]ethyl}benzoic acid (**5d**).* Following the procedure described for **5a**, compound **5d** was prepared from compound **4d** and 4-(2-hydroxyethyl)benzoic acid. The crude mixture was purified by preparative TLC (10% MeOH/DCM + 1% formic acid) to obtain the title compound as a white solid (30 mg, 0.061 mmol, 21%). ^{1}H-NMR (600 MHz, $(CD_3)_2SO$): δ 12.87 (1H, br), 12.18 (1H, br), 9.56 (1H, t, J = 6.0 Hz), 7.92-7.88 (2H, m), 7.85-7.81 (1H, m), 7.58-7.56 (1H, m), 7.51-7.49 (2H, m), 7.30-7.28 (1H, m), 7.24-7.22 (1H, m), 7.14-7.11 (1H, m), 4.46 (2H, d, J = 6 Hz), 4.36 (2H, t, J = 6 Hz), 3.22 (2H, t, J = 6 Hz), 2.26 (3H, d, J = 6 Hz) ppm. ^{13}C-NMR (150 MHz, $(CD_3)_2SO$): δ 167.3, 159.8 (d, J = 240 Hz), 159.4, 158.8, 153.8 (d, J = 245 Hz), 145.3, 145.2, 145.1, 143.6, 134.6 (d, J = 4.5 Hz), 130.8 (d, J = 6.0 Hz), 129.3, 129.2, 128.8, 126.8 (d, J = 9 Hz), 124.3 (d, J = 7.5 Hz), 123.9 (d, J = 17 Hz), 123.1 (d, J = 21 Hz), 118.2, 114.7 (d, J = 23 Hz), 75.2 (d, J = 1.5 Hz), 42.0, 35.8, 14.2 (d, J = 3.0 Hz) ppm. HRMS (ESI+, m/z): calculated $[M+Na]^+$ $C_{26}H_{21}F_2N_3O_5Na$ as 516.1347, found as 516.1365.

*6-Fluoro-5-[2-(4-methoxyphenyl)ethoxy]-N-[(4-methoxyphenyl)methyl]-4-oxo-3,4-dihydroquinazoline-2-carboxamide (**5e**).* Following the procedure described for **5a**, compound **5e** was prepared from compound **4c** and 2-(4-methoxyphenyl)ethanol. The crude mixture was purified by preparative TLC (20% EtOAc/hexane + 1% formic acid) to obtain the title compound as a white solid (42 mg, 0.088 mmol, 30%). ^{1}H-NMR (600 MHz, $(CD_3)_2SO$): δ 12.10 (1H, br), 9.44 (1H, t, J = 6.4 Hz), 7.80-7.77 (1H, m), 7.52-7.50 (1H, m), 7.28-7.26 (2H, m), 7.23-7.20 (2H, m), 6.90-6.87 (2H, m), 6.85-6.82 (2H,m), 4.39 (2H, d, J = 6.4 Hz), 4.22 (2H, t, J = 7.3 Hz), 3.72 (3H, s), 3.71 (3H, s), 3.02 (2H, t, J = 7.3 Hz) ppm. ^{13}C-NMR (150 MHz, $(CD_3)_2SO$): δ 159.2, 158.8, 158.8, 158.4, 157.8, 153.8 (d, J = 244 Hz), 145.4, 145.3, 145.2, 130.7, 129.9, 129.8, 129.0, 124.1 (d, J = 7.5 Hz) 123.1 (d, J = 22Hz), 118.2, 113.7, 75.9, 55.1, 55.0, 42.1, 34.9 ppm. HRMS (ESI+, m/z): calculated $[M+Na]^+$ $C_{26}H_{24}FN_3O_5Na$ as 500.1598, found as 500.1602.

*6-Fluoro-N-[(4-fluoro-3-methylphenyl)methyl]-5-[2-(4-methoxyphenyl)ethoxy]-4-oxo-3,4-dihydroquinazoline-2-carboxamide (**5f**).* Following the procedure described for **5a**, compound **5f** was prepared from compound **4d** and 2-(4-methoxyphenyl)ethanol. The crude mixture was purified by preparative TLC (30% EtOAc/hexane + 1% formic acid) to obtain the title compound as a white solid (40 mg, 0.083 mmol, 29%). ^{1}H-NMR (600 MHz, $(CD_3)_2SO$): δ 12.10 (1H, s), 9.51 (1H, t, J = 6.2 Hz), 7.80-7.77 (1H, m), 7.53-7.51 (1H, m), 7.25-7.24 (1H, m), 7.23-7.20 (2H, m), 7.19-7.17 (1H, m), 7.09-7.06 (1H, m), 6.85-6.83 (2H, m), 4.41 (2H, d, J = 6.2 Hz), 4.22 (2H, t, J = 7.3 Hz), 3.71 (3H, s), 3.03 (2H, t, J = 7.3 Hz), 2.21 (3H, d, J = 1.7 Hz) ppm. ^{13}C-NMR (150 MHz, $(CD_3)_2SO$): δ 159.8 (d, J = 240 Hz), 159.4, 158.8, 157.8, 153.8 (d, J = 244 Hz), 145.4 (d, J = 14 Hz), 145.3, 145.2, 134.6 (d, J = 3.0 Hz), 130.8 (d, J = 4.5 Hz), 129.9, 129.8, 126.8 (d, J = 8.3 Hz), 124.1 (d, J = 7.0 Hz), 123.9 (d, J = 18 Hz), 123.1 (d, J = 21 Hz), 118.2, 114.7 (d, J = 23 Hz),

113.7, 75.9, 55.0, 42.0, 34.9, 14.2 (d, J = 3.0 Hz) ppm. HRMS (ESI+, m/z): calculated $[M+Na]^+$ $C_{26}H_{23}F_2N_3O_4Na$ as 502.1554, found as 502.1581.

*6-Fluoro-5-[2-(4-hydroxyphenyl)ethoxy]-N-[(4-methoxyphenyl)methyl]-4-oxo-3,4-dihydroquinazoline-2-carboxamide (**5g**).* Following the procedure described for **5a**, compound **5g** was prepared from compound **4c** and 2-(4-hydroxyphenyl)ethanol. The crude mixture was purified by preparative TLC (30% EtOAc/hexane + 1% formic acid) to obtain the title compound as a white solid (24mg, 0.052 mmol, 18%). ^{1}H-NMR (600 MHz, $(CD_3)_2SO$): δ 12.09 (1H, br), 9.44 (1H, t, J = 6.4 Hz), 9.19 (1H, s), 7.80-7.77 (1H, m), 7.52-7.50 (1H, m), 7.28-7.26 (2H, m), 7.09-7.07 (2H, m), 6.89-6.88 (2H, m), 6.67-6.65 (2H, m), 4.39 (2H, d, J = 6.4 Hz), 4.18 (2H, t, J = 7.4 Hz), 3.72 (3H, s), 2.97 (2H, t, J = 7.4 Hz) ppm. ^{13}C-NMR (150 MHz, $(CD_3)_2SO$): δ 159.2, 158.8, 158.4, 155.7, 153.8 (d, J = 244 Hz), 145.4, 145.3, 145.3, 130.7, 129.8, 129.0, 127.8, 124.1 (d, J = 7.2 Hz), 123.1 (d, J = 21 Hz), 118.2, 115.1, 113.7, 76.1, 55.1, 42.1, 35.0 ppm. HRMS (ESI+, m/z): calculated $[M+Na]^+$ $C_{25}H_{22}FN_3O_5Na$ as 486.1441, found as 486.1452.

*6-Fluoro-N-[(4-fluoro-3-methylphenyl)methyl]-5-[2-(4-hydroxyphenyl)ethoxy]-4-oxo-3,4-dihydroquinazoline-2-carboxamide (**5h**).* Following the procedure described for **5a**, compound **5h** was prepared from compound **4d** and 2-(4-hydroxyphenyl)ethanol. The crude reaction mixture was purified by preparative TLC (30% EtOAc/hexane + 1% formic acid) to obtain the title compound as a white solid (26 mg, 0.056 mmol, 19%). ^{1}H-NMR (600 MHz, $(CD_3)_2SO$): δ 12.10 (1H, br), 9.51 (1H, t, J = 6.3 Hz), 9.19 (1H, s), 7.80-7.77 (1H, m), 7.52-7.51 (1H, m), 7.25-7.23 (1H, m), 7.20-7.17 (1H, m), 7.09-7.06 (3H, m), 6.67-6.65 (2H, m), 4.41 (2H,d, J = 6.4 Hz), 4.18 (2H, t, J = 7.4 Hz), 2.97 (2H, t, J = 7.4 Hz), 2.21 (3H, d, J = 1.8 Hz) ppm. ^{13}C-NMR (150 MHz, $(CD_3)_2SO$): δ 159.8 (d, J = 240 Hz), 159.4, 158.8, 155.8, 153.8 (d, J = 244 Hz), 145.4, 145.3, 145.2 134.6 (d, J = 3.4 Hz), 130.8 (d, J = 5.3 Hz), 129.8, 127.8, 126.8 (d, J = 7.9 Hz) 124.1 (d, J =

7.0 Hz), 123.9 (d, J = 17 Hz), 123.1 (d, J = 21 Hz), 118.2, 115.1, 114.7 (d, J = 22 Hz), 76.1, 42.0, 34.9, 14.2 (d, J = 3.2 Hz) ppm. HRMS (ESI+, m/z): calculated $[M+Na]^+$ $C_{25}H_{21}F_2N_3O_4Na$ as 488.1398, found as 488.1419.

*6-Fluoro-5-(2-fluoroethoxy)-N-[(4-methoxyphenyl)methyl]-4-oxo-3,4-dihydroquinazoline-2-carboxamide (**5i**).* Following the procedure described for **5a**, compound **5i** was prepared from compound **4c** and 2-fluoroethanol. The crude mixture was purified by preparative TLC (20% EtOAc/hexane + 1% formic acid) to obtain the title compound as a white solid (30 mg, 0.077 mmol, 27%). ^{1}H-NMR (600 MHz, $(CD_3)_2SO$) δ 12.16 (1H, br), 9.45 (1 H, t, J = 6.2 Hz), 7.83-7.80 (1H, m), 7.56-7.54 (1H, m), 7.28-7.26 (2H, m), 6.90-6.87 (2H, m), 4.78-4.69 (2H, m), 4.39 (2H, d, J = 6.4 Hz), 4.36-4.30 (2H, m), 3.72 (3H, s) ppm. ^{13}C-NMR (150 MHz, $(CD_3)_2SO$): δ 159.2, 158.8, 158.4, 153.8 (d, J = 245 Hz), 145.3, 145.2, 145.1, 130.7, 129.0, 124.5 (d, J = 7.5 Hz), 123.1 (d, J = 22 Hz), 118.1, 113.7, 83.1 (d, J = 166 Hz), 74.4 (d, J = 18 Hz), 55.1, 42.1 ppm. HRMS (ESI+, m/z): calculated $[M+Na]^+$ $C_{19}H_{17}F_2N_3O_4Na$ as 412.1085, found as 412.1098.

*6-Fluoro-N-[(4-fluoro-3-methylphenyl)methyl]-5-(2-fluoroethoxy)-4-oxo-3,4-dihydroquinazoline-2-carboxamide (**5j**).* Following the procedure described for **5a**, compound **5j** was prepared from compound **4d** and 2-fluoroethanol. The crude mixture was purified by preparative TLC (20% EtOAc/hexane + 1% formic acid) to obtain the title compound as a white solid (29 mg, 0.074 mmol, 26%). ^{1}H-NMR (600 MHz, $(CD_3)_2SO$): δ 12.17 (1H, s), 9.52 (1H, t, J = 6.2 Hz), 7.84-7.80 (1H, m), 7.56-7.54 (1H, m), 7.25-7.24 (1H, m), 7.20-7.17 (1H, m), 7.09-7.06 (1H, m), 4.78-4.69 (2H, m), 4.41 (2H, d, J = 6.4 Hz), 4.36-4.30 (2H, m), 2.21 (3H, d, J = 1.7 Hz) ppm. ^{13}C-NMR (150 MHz, $(CD_3)_2SO$): δ 159.8 (d, J = 240 Hz), 159.4, 158.8, 153.8 (d, J = 245 Hz), 145.3, 145.2, 145.0 (d, J = 14 Hz), 134.6 (d, J = 3.3 Hz), 130.8 (d, J = 4.7 Hz), 126.8 (d, J =

8.3 Hz), 124.5 (d, J = 6.5 Hz), 123.9 (d, J = 17 Hz), 123.1 (d, J = 21 Hz), 118.1, 114.7 (d, J = 22 Hz), 83.1 (d, J = 165 Hz), 74.4 (d, J = 19 Hz), 42.0, 14.2 (d, J = 3.3 Hz) ppm. HRMS (ESI+, m/z): calculated $[M+Na]^+$ $C_{19}H_{16}F_3N_3O_3Na$ as 414.1041, found as 414.1056.

*2-[(Tetrahydro-2H-pyran-2-yl)oxy]ethan-1-ol (**6**).* To a solution of *p*-toluenesulfonic acid monohydrate (312 mg, 1.64 mmol, 5 mol%) in ethylene glycol (14.0 mL, 250 mmol, 7.6 equiv.) was added dihydropyran (3.00 mL, 32.9 mmol, 1.0 equiv.) dropwise over 30 min at 0 °C. The solution was stirred at 0 °C for 2 h and then at room temperature for an additional 4 h. The reaction was then diluted with DCM and extracted with 0.1 M NaOH. The combined organics were dried over Na_2SO_4, filtered, and concentrated under reduced pressure. The crude mixture was purified by column chromatography (0-50% EtOAc/hexane) to obtain the title compound as a colorless oil (3.80 g, 26.0 mmol, 79%). ^{1}H-NMR (600 MHz, $CDCl_3$): δ 4.56-4.55 (1H, m), 3.93-3.89 (1H, m), 3.78-3.67 (4H, m), 3.55-3.51 (1H, m), 2.90 (1H, br), 1.85-1.80 (1H, m), 1.77-1.73 (1H, m), 1.60-1.50 (4H, m) ppm. ^{13}C-NMR (150 MHz, $CDCl_3$): δ 100.3, 70.9, 63.4, 62.4, 30.9, 25.3, 20.1 ppm. HRMS (EI, m/z): $[M-H]^+$ calculated $C_7H_{14}O_3$ as 145.0859, found as 145.0846. Spectrum in accordance with literature.[43]

6-Fluoro-N-[(4-fluoro-3-methylphenyl)methyl]-5-[2-(oxan-2-yloxy)ethoxy]-4-oxo-3,4-dihydroquinazoline-2-carboxamide (7). Following the procedure described for **5a**, compound **7** was prepared from compound **4d** and compound **6**. The crude mixture was purified by column chromatography (0-40% EtOAc/hexane) to obtain the title compound as a white solid (376 mg, 0.79 mmol, 75%). ^{1}H-NMR (600 MHz, $(CD_3)_2SO$): δ 12.14 (1H, br), 9.55 (1H, t, J = 6.0 Hz), 7.84-7.81 (1H, m), 7.57-7.55 (1H, m), 7.29-7.27(1H, m), 7.23-7.21 (1H, m), 7.13-7.10 (1H, m), 4.65-4.63 (1H, m), 4.45 (2H, d, J = 6.0 Hz), 4.32-4.25 (2H, m), 3.96-3.93 (1H, m), 3.78-3.72 (2H, m), 3.45-3.36 (1H, m), 2.24 (3H, d, J = 6.0 Hz), 1.68-1.55 (2H, m), 1.51-1.36 (4H, m). ^{13}C-NMR (150

MHz, $(CD_3)_2SO$) 159.8 (d, J = 240 Hz), 159.4, 158.9, 153.8 (d, J = 245 Hz), 145.7 (d, J = 14 Hz), 145.3, 145.2, 134.6 (d, J = 4.5 Hz), 130.8 (d, J = 4.5 Hz), 126.9 (d, J = 7.5 Hz), 124.1, 123.9 (d, J = 17 Hz), 123.0 (d, J = 23 Hz), 118.1, 114.7 (d, J = 21 Hz), 98.0, 74.4 (d, J = 3.0 Hz), 66.4, 61.1, 42.1, 30.1, 25.0, 18.9, 14.2 (d, J = 3.0 Hz) ppm. HRMS (ESI+, m/z): calculated $[M+Na]^+$ $C_{24}H_{25}F_2N_3O_5Na$ as 496.1660, found as 496.1653.

6-Fluoro-N-[(4-fluoro-3-methylphenyl)methyl]-5-(2-hydroxyethoxy)-4-oxo-3,4-dihydroquinazoline-2-carboxamide (8). To a solution of compound **7** (376 mg, 0.79 mmol, 1.0 equiv.) in MeOH (7.94 mL) was added *p*-toluenesulfonic acid monohydrate (12.2 mg, 0.064 mmol, 8 mol%). The solution was stirred at room temperature for 1 h before removal of the solvent under reduced pressure. The residue was re-suspended in DCM and extracted with water. The combined organics were dried over Na_2SO_4, filtered, and concentrated under reduced pressure. The crude mixture was purified by column chromatography (20-60% EtOAc/hexane) to obtain the title compound as a white solid (230 mg, 0.59 mmol, 75%). ^{1}H-NMR (600 MHz, $(CD_3)_2SO$): δ 12.27 (1H, br), 9.56 (1H, t, J = 6.0 Hz), 7.87-7.84 (1H, m), 7.59-7.57 (1H, m), 7.29-7.27 (1H, m), 7.24-7.21 (1H, m), 7.13-7.10 (1H, m) 4.95 (1H, t, J = 6.0 Hz), 4.45 (2H, d, J = 6.0 Hz), 4.20 (2H, t, J = 6.0 Hz), 3.76 (2H, q, J = 6.0 Hz), 2.25 (3H, d, J = 6.0 Hz) ppm. ^{13}C-NMR (150 MHz, $(CD_3)_2SO$): δ 159.8 (d, J = 240 Hz), 159.7, 159.3, 153.8 (d, J = 245 Hz), 145.7 (d, J = 14 Hz), 145.3, 145.1, 134.6 (d, J = 3.0 Hz), 130.8 (d, J = 4.5 Hz), 126.8 (d, J = 9.0 Hz), 124.0, 123.9 (d, J = 18 Hz), 123.3 (d, J = 21 Hz), 117.7, 114.7 (d, J = 21 Hz), 77.0 (d, J = 3.0 Hz), 60.2, 42.1, 14.2 (d, J = 3.0 Hz) ppm. HRMS (ESI+, m/z): calculated $[M+Na]^+$ $C_{19}H_{17}F_2N_3O_4Na$ as 412.1085, found as 412.1069.

*2-[(6-Fluoro-2-{[(4-fluoro-3-methylphenyl)methyl]carbamoyl}-4-oxo-3,4-dihydroquinazolin-5-yl)oxy]ethyl 4-methylbenzene-1-sulfonate (**9**).* To a solution of compound **8**

(200 mg, 0.51 mmol, 1.0 equiv.) in pyridine (1.14 mL) was added *p*-toluenesulfonyl chloride (294 mg, 1.54 mmol, 3.0 equiv.) portionwise at 0 °C over 30 min. The solution was stirred for 4 h at 0 °C, diluted with EtOAc and extracted with 1 M HCl followed by water. The combined organics were dried over Na_2SO_4, filtered, and concentrated under reduced pressure. The crude mixture was purified by column chromatography (20-70% EtOAc/hexane) to obtain the title compound as a white solid (233 mg, 0.43 mmol, 84%). ^{1}H-NMR (600 MHz, $(CD_3)_2SO$): δ 12.19 (1H, br), 9.57 (1H, t, J = 6.0 Hz), 7.84-7.81 (1H, m), 7.78-7.76 (2H, m), 7.59-7.57 (1H, m), 7.48-7.46 (2H, m), 7.29-7.28 (1H, m), 7.24-7.21 (1H, m), 7.13-7.10 (1H, m), 4.45 (2H, d, J = 6.0 Hz) 4.40-4.39 (2H, m), 4.30-4.29 (2H, m), 2.42 (3H, s), 2.25 (3H, d, J = 6.0 Hz) ppm. ^{13}C-NMR (150 MHz, $(CD_3)_2SO$): δ 159.8 (d, J = 240 Hz), 159.4, 158.8, 153.6 (d, J = 246 Hz), 145.3, 145.2 145.0, 144.7 (d, J = 14 Hz), 134.6 (d, J = 4.5 Hz), 132.2, 130.8 (d, J = 6.0 Hz), 130.1, 127.6, 126.9 (d, J = 9.0 Hz), 124.6, 123.9 (d, J = 17 Hz), 123.2 (d, J = 23 Hz), 117.9, 114.7 (d, J = 23 Hz), 72.5 (d, J = 1.5 Hz), 70.2, 42.1, 21.1, 14.2 (d, J = 3.0 Hz) ppm. HRMS (ESI+, m/z): calculated $[M+Na]^+$ $C_{26}H_{23}F_2N_3O_6SNa$ as 566.1173, found as 566.1166.

*2-{[1-(Dimethylamino)-7-fluoro-2-[(4-fluoro-3-methylphenyl)methyl]-3,9-dioxo-1H,2H,3H,9H-imidazo[4,3-b]quinazolin-8-yl]oxy}ethyl 4-methylbenzene-1-sulfonate (**10**).* To a solution of compound **9** (71 mg, 0.13 mmol, 1.0 equiv.) in anhydrous DMF (0.20 mL) and THF (0.42 mL) was added oxalyl chloride (33 uL, 0.39 mmol, 3.0 equiv.) dropwise at 0 °C. The solution was stirred at room temperature for 2 h before removal of the solvent under reduced pressure. The residue was re-suspended in EtOAc and extracted with water. The combined organics were dried over Na_2SO_4, filtered, and concentrated under reduced pressure. The crude mixture was purified by column chromatography (0-60% EtOAc/hexane) to obtain the title compound as a bright yellow solid (66 mg, 0.11 mmol, 85%). ^{1}H-NMR (600 MHz, $(CD_3)_2SO$): δ 7.90-7.86 (1H, m), 7.78 (2H,

d, J = 8.2 Hz), 7.71-7.69 (1H, m), 7.47 (2H, d, J = 8.2 Hz), 7.33-7.30 (1H, m), 7.27-7.23 (1H, m), 7.17-7.14 (1H, m), 6.15 (1H, s), 4.87 (1H, d, J = 15 Hz), 4.42-4.28 (5H, m), 2.43 (3H, s), 2.34 (6H, br), 2.26 (3H, s) ppm. ^{13}C-NMR (150 MHz, $CDCl_3$): δ 161.4 (d, J = 245 Hz), 157.4, 157.3, 154.8 (d, J = 250 Hz), 146.5, 145.8 (d, J = 14 Hz), 145.0, 144.4, 133.0, 132.3 (d, J = 6.0 Hz), 130.5 (d, J = 3.0 Hz), 129.9, 128.2, 128.1, 126.0 (d, J = 7.5 Hz), 125.9 (d, J = 18 Hz), 123.6 (d, J = 21 Hz), 117.6, 115.6 (d, J = 23 Hz), 105.8, 87.0, 72.6 (d, J = 3.0 Hz), 68.9, 43.2, 21.8, 14.7 ppm. HRMS (ESI+, m/z): calculated $[M+Na]^+$ $C_{29}H_{28}F_2N_4O_6SNa$ as 621.1595, found as 621.1578.

MMP Enzyme Inhibition Assay

Inhibitor potency against human recombinant MMP-1,-2,-8,-9, and -13 (R&D Systems) was measured using the fluorogenic substrate Mca-Lys-Pro-Leu-Gly-Leu-Dpa-Ala-Arg-NH_2 (Sigma Aldrich, MMP-13 K_M = 5.2 μM)[48] or Mca-Arg-Pro-Lys-Pro-Val-Glu-Nval-Trp-Arg-Lys(Dnp)-NH_2 (R&D Systems) for human recombinant MMP-10 (R&D Systems). Enzymes were activated with *para*-aminophenylmercuric acetate (1 mM) at 37 °C for the time indicated by the provider and diluted in assay buffer (pH 7.5) containing Tris (50 mM), NaCl (0.15 M), $CaCl_2$ (5 mM), $ZnSO_4$ (20 μM) and Brij 35 (0.05% w/v). Inhibitor solutions (45 μL) were prepared in DMSO, diluted to varying concentrations spanning 2 orders of magnitude in assay buffer (<5% DMSO final), and incubated with the active enzyme (45 μL, 4.44 nM) at 37°C for 30 min. The reaction was initiated with the addition of substrate (10 μL, 50 μM). Final concentrations of the enzyme and substrate were 2 nM and 5 μM, respectively. Changes in fluorescence were monitored using a BioTek Synergy Mx multi-mode plate reader with excitation and emission wavelengths of 320 and 405 nm, respectively. Initial rates were measured over the linear range (0-10 min), normalized to the observed reaction rates for no enzyme (0% activity) and no inhibitor (100% activity) control wells, and plotted as a function of inhibitor concentration on a logarithmic scale.

The IC_{50} values were calculated by nonlinear regression analysis according to the following equation using GraphPad Prism software:

$$Y = \frac{100}{1+10^{(\mathrm{LogIC_{50}}-X)*\mathrm{HillSlope}}} \qquad (1)$$

Radiochemistry

*Automated Radiosynthesis – [^{11}C]**5b.*** A fully automated sequence including the generation of [^{11}C]CH_3I and radiolabeling were performed on a Synthra MeIPlus Research system. [^{11}C]CO_2 was prepared on a Siemens CTI Eclipse HP/RD Hybrid Cyclotron (11 MeV) via the $^{14}N(p,\alpha)^{11}C$ nuclear reaction. [^{11}C]CO_2 (~27 GBq) was transferred from the target, delivered into the module, and trapped on a steel coil at -180 °C. The trap was then heated to 50 °C, [^{11}C]CO_2 was released by H_2 gas flow (40 mL·min^{-1}) and reduced using a nickel catalyst (99.999% purity, C < 100 ppm) at 425 °C. The generated [^{11}C]CH_4 was trapped on a Carboxen® column (60-80 mesh) at -140 °C. The trap was then heated to 160 °C, [^{11}C]CH_4 was released by He gas flow (100 mL·min^{-1}), directed over iodine at 95 °C (99.999% purity, -10 mesh, anhydrous beads) and heated in a high temperature oven at 720 °C. The generated [^{11}C]CH_3I was trapped on a Porapak™ Q column (50-80 mesh), while unreacted [^{11}C]CH_4 was re-circulated in a closed system with a gas pump. When conversion was complete, the Porapak™ Q column was heated at 200 °C, [^{11}C]CH_3I was released by He gas flow (30 mL·min^{-1}) and bubbled into the reactor containing precursor (10 mM) and TBAOH (6.29 µL, 3 equiv.) dissolved in anhydrous DMSO (209 µL). The reactor was then heated at 80°C for 3 min, immediately cooled to 30 °C, and quenched with water (500 µL). The crude mixture was purified with a Phenomenex Synergi Hydro-RP column (C18, 80Å, 10 µm, 250 mm × 10 mm), mobile phase: 65/35 0.1 M ammonium formate / ACN (isocratic), flowrate: 5 mL·min^{-1}. The product fraction (retention time: ~9.5 min) was collected into a bulk vessel containing water (40 mL). The contents of the flask were transferred over a Waters Sep-Pak Plus Short C18 cartridge

(preconditioned with 1 mL EtOH, 5 mL water, and 1 mL air) and subsequently washed with water (10 mL). The product was eluted with EtOH (1 mL) and diluted with saline (9 mL, 0.9%).

*Automated Radiosynthesis – [^{11}C]**5f***. An automated synthesis of **[^{11}C]5f** was performed according to the procedure described for **[^{11}C]5b** with TBAOH (4.19 µL, 2 equiv.). The crude mixture was purified with a Phenomenex Synergi Hydro-RP column (C18, 80Å, 10 µm, 250 mm × 10 mm), mobile phase: 35/65 0.1 M ammonium formate / ACN (isocratic), flowrate: 5 mL·min^{-1}. The product fraction (retention time: ~11 min) was collected and reformulated in 10% EtOH/saline (0.9%).

*Automated Radiosynthesis – [^{18}F]**5j***. A fully automated sequence was developed on a GE TRACERlab FX2N automation system. No-carrier-added aqueous [^{18}F]fluoride was prepared on a Siemens CTI Eclipse HP/RD Hybrid Cyclotron (11 MeV) via the ^{18}O(p,n)^{18}F nuclear reaction. [^{18}F]Fluoride (~13 GBq) was captured from the [^{18}O]H_2O target solution using a Waters Sep-Pak Light Accell Plus QMA Cartridge (preconditioned with 10 mL EtOH, 10 mL water, 10 mL 0.5 M $NaHCO_3$, 10 mL water, and 1 mL air) and eluted into the reactor with aqueous tetraethylammonium bicarbonate (800µL 3.23 mg/mL). Anhydrous ACN (1 mL) was also added and the reactor was heated at 80 °C for 5 min and 120 °C for 3 min under a nitrogen stream to yield dried [^{18}F]TEAF. The reactor was then cooled to 40 °C with compressed air, before adding the precursor (3.66 mg) in anhydrous DMSO (500 µL). The radiofluorination was performed at 100 °C for 10 min, and returned to 50 °C. Subsequently, hydrochloric acid (6M, 500 µL) was added and the deprotection was performed at 100 °C for 10 min. Following cooling with compressed air, the reaction was quenched with sodium hydroxide (6M, 400 µL) and HPLC mobile phase (1 mL) and loaded onto the HPLC loop. The crude mixture was purified with a Phenomenex Synergi Hydro-RP column (C18, 80Å, 10 µm, 250 mm × 10 mm), mobile phase: 50% 0.1 M

ammonium formate / ACN (isocratic), flowrate: 5 mL·min^{-1}. The product fraction (retention time: ~15 min) was collected into a bulk vessel containing water (25 mL). The contents of the flask were transferred over a Waters Sep-Pak Plus Short C18 cartridge (preconditioned with 1 mL EtOH, 5 mL water, and 1 mL air) and subsequently washed with water (10 mL). The product was eluted with EtOH (1 mL) and diluted with saline (9 mL, 0.9%).

*Manual Optimization – [^{11}C]**5b** and [^{11}C]**5f**.* ^{11}C-Methylation conditions were optimized on the Synthra MeIPlus Research system. [^{11}C]CH_3I was generated as previously described and bubbled into the reactor containing precursor (0.5 mg) and the indicated amount of TBAOH (1-4 equiv.) dissolved in anhydrous DMSO (10 mM). The reactor was then heated at the indicated temperature for the indicated time, immediately cooled to 30 °C, and quenched with water (250 µL). The crude reaction mixture was transferred to a sealed vial and analyzed by radio-HPLC using the conditions in the radiotracer quality control section. Radiochemical conversion was defined as the percentage of total radioactivity corresponding to the desired product (decay-corrected). Radiochemical identity was confirmed by co-injection of the corresponding non-radioactive standard.

*Manual Optimization – [^{18}F]**5j**.* Radiofluorination conditions were manually optimized in sealed conical vials. Azeotropic drying of aqueous [^{18}F]fluoride (~37 MBq) containing the indicated amount of base (1-8 equiv.), and anhydrous ACN (3 × 1 mL) was performed at 100 °C under nitrogen gas dried over a P_2O_5 column. A solution of the precursor (13.5 mM) in anhydrous DMSO (250 µL) was then added and the reaction mixture was heated at the indicated temperature (100 or 120 °C). Samples were withdrawn for radio-TLC analysis after 10, and 20 min, spotted on a silica-coated TLC plate, and developed in a chamber containing EtOAc until the solvent front reached 2 cm from the top of the plate. Incorporation of [^{18}F]fluoride was quantified using a

Bioscan AR-2000 radio-TLC imaging scanner and WinScan software by integration of product peaks and unreacted [^{18}F]fluoride. Quantitative deprotection was observed with hydrochloric acid (6M, 500 μL) at 100°C for 10 min by radio-HPLC using the conditions in the radiotracer quality control section. Radiochemical identity was confirmed by co-injection of the corresponding non-radioactive standard.

*Radiotracer Quality Control – [^{11}C]**5b**, [^{11}C]**5f**, and [^{18}F]**5j**.* Radiochemical purity and identity were confirmed by analytical radio-HPLC using a Phenomenex Luna C18 column (100 Å, 5 μm, 250 mm × 4.6 mm), a 996 Photodiode Array Detector (PerkinElmer), and a Carroll & Ramsey Associates 105-S high-sensitivity radiation detector. HPLC solvent A: 0.1 M ammonium formate, HPLC solvent B: ACN, flowrate: 1 mL·min^{-1}. **[^{11}C]5b** method: 0-2 min 25% B, 2-10 min 25-95% B, 10-12 min 95% B, 12-13 min 95-25% B, 13-15 25% B, retention time: 9.5 min. **[^{11}C]5f** method: 0-2 min 50% B, 2-8 min 50-95% B, 8-10 min 95% B, 10-13 min 95-50% B, 13-15 min 50% B, retention time: 9.5 min. **[^{18}F]5j** method: 0-2 min 20% B, 2-10 min 20-90% B, 10-12 min 90% B, 12-13 min 90-20% B, 13-15 min 20% B, retention time: 11.5 min. Molar activity was determined by measuring the UV absorbance of a known amount of radioactivity under identical HPLC conditions used to generate a calibration curve for the corresponding non-radioactive standard. The ratio of radioactivity (GBq) to moles (μmol) provided the molar activity (GBq·μmol^{-1}), which was decay corrected to the end of synthesis (EoS).

Formulation Stability

Radiotracer stability in 10% EtOH/saline (0.9%) was assessed at room temperature up to 75 min by analytical radio-HPLC using the conditions described in the radiotracer quality control section. Radiochemical purity was >99% for all radiotracers immediately following reformulation.

Distribution Coefficient (logD)

Radiotracer lipophilicity was measured by determination of the 1-octanol - 1× PBS (pH 7.4) distribution coefficient (logD) as previously described[49]. Data represent the mean ± standard error of two independent experiments performed in quadruplicate.

Animal Model

Male *ApoE*$^{-/-}$ (strain no. 002052) mice were obtained from Jackson Laboratory and housed in groups of 4. Mice were fed a western atherogenic diet (TD.88137, Envigo) beginning at 8 weeks of age for a total of 13-16 weeks. Animals were monitored periodically and housed in environmentally enriched cages with free access to food and water. All housing, handling, and experimental procedures were in strict accordance with the guidelines of Canadian Council on Animal Care and with approval of the University of Ottawa Animal Care Committee.

PET Imaging

ApoE$^{-/-}$ mice (41 ± 2 g, n = 2 per group) were anesthetized with 2% isoflurane, positioned in the PET scanner, and maintained under anesthesia during the imaging protocol. Following a 10 min transmission scan, animals were intravenously injected with radiotracer (~7.5 MBq) as a bolus over 30 sec via the lateral tail vein. The whole body was imaged for 60 min (4 × 15 sec frames; 4 × 1 min frames; 11 × 5 min frames). PET imaging was performed using a Siemens DPET scanner. Emission data were corrected for attenuation and scatter, then reconstructed using the 3D-OSEM/MAP algorithm. Volumetric regions of interest (ROIs) were drawn over target organs. Uptake values obtained in nCi·cc^{-1} were converted to %ID·cc^{-1} using the injected dose (nCi) and presented as time-activity curves.

Biodistribution

ApoE$^{-/-}$ mice (39 ± 5 g, n = 4-6 per group) were anesthetized with 2% isoflurane and intravenously injected with radiotracer (~7.5 MBq, 100-200 μL) as a bolus over 30 sec via the lateral tail vein. For pharmacological treatments, **5j** (2.5 mg/kg, 3 mg/mL, 16% DMA/ 32% propylene glycol/ 32% PEG400/ 20% sterile water), or WAY170523 (7.5 mg/kg, 3.5 mg/mL, 10% DMSO, 40% PEG400, 50% sterile water), were intravenously administered 15 min prior to the radiotracer. Isoflurane was maintained for 30 min, blood was collected by cardiac puncture, and animals were sacrificed by myocardial perfusion (10 mL 1× PBS, 10 mL 10% formalin, 5 mL 1× PBS). Perfusate was drained from an incision within the right atrium. Organs of interest were harvested, weighed, and counted for radioactivity using a Hidex Automatic Gamma Counter (energy window: 480−558 keV). Counts per minute (CPM) were converted to activity using a set of calibration standards with known activities. Percentage injected dose (%ID) was calculated by dividing the organ activity by the injected dose (decay-corrected) and further normalized by sample mass (g) to obtain the percentage injected dose per gram tissue (%ID/g).

Plasma Radio-Metabolite Analysis

Blood samples were withdrawn by cardiac puncture into K_2EDTA-coated blood collection tubes 30 minutes after intravenous radiotracer administration. Protein-free plasma samples were obtained as previously described.[25] Pooled plasma samples were then spiked with non-radioactive standard and analyzed by radio-HPLC using the analytical methods described in the radiotracer quality control section. Fractions were collected each minute and counted for radioactivity using a gamma counter. Polar and non-polar radio-metabolites were defined by the radioactivity collected before and after the parent fraction, respectively. Extraction efficiency was defined as the percentage recovery of radioactivity in plasma following protein precipitation.

Autoradiography and Oil Red O Staining

Following removal of residual blood by myocardial perfusion, aortae and branching arteries were carefully dissected under a microscope and exposed to a super-resolution GE Storage Phosphor Screen (BAS-IP SR 2025 E) for 10 half-lives. The screen was scanned with a Cyclone Plus Storage Phosphor System and quantified using OptiQuant software by drawing aortic arch regions of interest (ROI) which were Oil Red O (ORO) positive. Digital light units (DLU) were converted to activity (Bq) using a set of calibration standards with known activities on the same screen. Percentage injected dose (%ID) was calculated by dividing the ROI activity (Bq) by the injected dose (Bq) and further normalized by ROI area (mm^2) to obtain ROI activity density ($\%ID \cdot mm^{-2}$). ORO staining was performed as previously described.[50] Bright-field images were taken using a Krüss Stereomicroscope (MSL4000-series) adapted with a smartphone camera and cropped.

Statistical Analysis

Statistical analysis was performed using GraphPad Prism. Data are presented as mean ± standard error. Multiple groups were compared using 1-way or 2-way ANOVA with Dunnett's or Tukey's multiple comparison test. Significance was set at the 0.05 level.

ASSOCIATED CONTENT

The supporting information is available free of charge on the ACS publications website at DOI:

^{1}H NMR and ^{13}C NMR spectra for all synthesized compounds; characterization of S_NAr selectivity; UPLC traces for **5b**, **5f** and **5j;** Representative radio-HPLC chromatograms following

isolation of **[^{11}C]5b**, **[^{11}C]5f**, and **[^{18}F]5j**; Stability of **[^{11}C]5b**, **[^{11}C]5f**, and **[^{18}F]5j** in formulation; **[^{18}F]5j** blood clearance time-course; (PDF). Molecular formula strings; (CSV).

AUTHOR INFORMATION

Corresponding author

Benjamin H. Rotstein; Phone: 613-696-7324; Email: benjamin.rotstein@uottawa.ca

Author contributions

A.B. and B.H.R. designed the project, directed research, performed experiments, analyzed data, and wrote the manuscript. J.W.K. guided enzyme inhibition assays. All other authors performed experiments. All authors approved of the manuscript.

Notes

The authors declare no competing financial interest.

ACKNOWLEDGMENTS

The authors thank the staff of the University of Ottawa Heart Institute (UOHI) PET Radiochemistry Laboratory, Biomedical Engineering, and Animal Care and Veterinary Services for cyclotron, PET scanner, and animal care support. Support for this work was provided by CIHR (PJT 148968), CFI (JELF 36848 & 39358), and the Ontario Ministry for Research, Innovation and Science (ER17-13-119). A.B. was supported by OGS, QEII-GSST, and a UOHI Endowed Research Scholarship. U.S.I. was supported by QEII-GSST and the University of Ottawa Cardiac Endowment Fund. M.A. was supported by NSERC USRA and University of Ottawa UROP.

ABBREVIATIONS USED

A_M, molar activity; ARG, autoradiography; CPM, counts per minute; DLU, digital light units; Dnp, 2,4-dinitrophenol; EoS, end-of-synthesis; %ID, percentage of injected dose; Mca, 7-methoxycoumarin-4-acetic acid; Nval, norvaline; OAT, organic anion transporter; ORO, Oil Red O; QMA, quaternary methyl ammonium; RCC, radiochemical conversion; RCY, radiochemical yield; ROI, region of interest; SEM, standard error of the mean; S_NAr, nucleophilic aromatic substitution; TBAOH, tetrabutylammonium hydroxide; TEAB, tetraethylammonium bicarbonate;

REFERENCES

(1) Loffek, S.; Schilling, O.; Franzke, C.-W. Biological Role of Matrix Metalloproteinases: A Critical Balance. *Eur. Respir. J.* **2011**, *38* (1), 191–208. https://doi.org/10.1183/09031936.00146510.

(2) Laronha, H.; Caldeira, J. Structure and Function of Human Matrix Metalloproteinases. *Cells* **2020**, *9* (5), 1076. https://doi.org/10.3390/cells9051076.

(3) Sternlicht, M. D.; Werb, Z. How Matrix Metalloproteinases Regulate Cell Behavior. *Annu. Rev. Cell Dev. Biol.* **2001**, *17*, 463–516. https://doi.org/10.1146/annurev.cellbio.17.1.463.

(4) Cabral-Pacheco, G. A.; Garza-Veloz, I.; Castruita-De la Rosa, C.; Ramirez-Acuña, J. M.; Perez-Romero, B. A.; Guerrero-Rodriguez, J. F.; Martinez-Avila, N.; Martinez-Fierro, M. L. The Roles of Matrix Metalloproteinases and Their Inhibitors in Human Diseases. *Int. J. Mol. Sci.* **2020**, *21* (24), 9739. https://doi.org/10.3390/ijms21249739.

(5) Klein, T.; Bischoff, R. Physiology and Pathophysiology of Matrix Metalloproteases. *Amino Acids* **2011**, *41* (2), 271–290. https://doi.org/10.1007/s00726-010-0689-x.

(6) Nissinen, L.; Kähäri, V.-M. Matrix Metalloproteinases in Inflammation. *Biochim. Biophys. Acta BBA - Gen. Subj.* **2014**, *1840* (8), 2571–2580. https://doi.org/10.1016/j.bbagen.2014.03.007.

(7) Kular, J. K.; Basu, S.; Sharma, R. I. The Extracellular Matrix: Structure, Composition, Age-Related Differences, Tools for Analysis and Applications for Tissue Engineering. *J. Tissue Eng.* **2014**, *5*, 2041731414557112. https://doi.org/10.1177/2041731414557112.

(8) Inada, M.; Wang, Y.; Byrne, M. H.; Rahman, M. U.; Miyaura, C.; López-Otín, C.; Krane, S. M. Critical Roles for Collagenase-3 (Mmp13) in Development of Growth Plate Cartilage and in Endochondral Ossification. *Proc. Natl. Acad. Sci. U. S. A.* **2004**, *101* (49), 17192–17197. https://doi.org/10.1073/pnas.0407788101.

(9) Yamamoto, K.; Okano, H.; Miyagawa, W.; Visse, R.; Shitomi, Y.; Santamaria, S.; Dudhia, J.; Troeberg, L.; Strickland, D. K.; Hirohata, S.; Nagase, H. MMP-13 Is Constitutively Produced in Human Chondrocytes and Co-Endocytosed with ADAMTS-5 and TIMP-3 by the Endocytic Receptor LRP1. *Matrix Biol.* **2016**, *56*, 57–73. https://doi.org/10.1016/j.matbio.2016.03.007.

(10) Wang, M.; Sampson, E. R.; Jin, H.; Li, J.; Ke, Q. H.; Im, H.-J.; Chen, D. MMP13 Is a Critical Target Gene during the Progression of Osteoarthritis. *Arthritis Res. Ther.* **2013**, *15* (1), R5. https://doi.org/10.1186/ar4133.
(11) Kamekura, S.; Hoshi, K.; Shimoaka, T.; Chung, U.; Chikuda, H.; Yamada, T.; Uchida, M.; Ogata, N.; Seichi, A.; Nakamura, K.; Kawaguchi, H. Osteoarthritis Development in Novel Experimental Mouse Models Induced by Knee Joint Instability. *Osteoarthritis Cartilage* **2005**, *13* (7), 632–641. https://doi.org/10.1016/j.joca.2005.03.004.
(12) Little, C. B.; Barai, A.; Burkhardt, D.; Smith, S. M.; Fosang, A. J.; Werb, Z.; Shah, M.; Thompson, E. W. Matrix Metalloproteinase 13-Deficient Mice Are Resistant to Osteoarthritic Cartilage Erosion but Not Chondrocyte Hypertrophy or Osteophyte Development. *Arthritis Rheum.* **2009**, *60* (12), 3723–3733. https://doi.org/10.1002/art.25002.
(13) Pivetta, E.; Scapolan, M.; Pecolo, M.; Wassermann, B.; Abu-Rumeileh, I.; Balestreri, L.; Borsatti, E.; Tripodo, C.; Colombatti, A.; Spessotto, P. MMP-13 Stimulates Osteoclast Differentiation and Activation in Tumour Breast Bone Metastases. *Breast Cancer Res.* **2011**, *13* (5), R105. https://doi.org/10.1186/bcr3047.
(14) Zhang, B.; Cao, X.; Liu, Y.; Cao, W.; Zhang, F.; Zhang, S.; Li, H.; Ning, L.; Fu, L.; Niu, Y.; Niu, R.; Sun, B.; Hao, X. Tumor-Derived Matrix Metalloproteinase-13 (MMP-13) Correlates with Poor Prognoses of Invasive Breast Cancer. *BMC Cancer* **2008**, *8*, 83. https://doi.org/10.1186/1471-2407-8-83.
(15) Sukhova, G. K.; Schönbeck, U.; Rabkin, E.; Schoen, F. J.; Poole, A. R.; Billinghurst, R. C.; Libby, P. Evidence for Increased Collagenolysis by Interstitial Collagenases-1 and -3 in Vulnerable Human Atheromatous Plaques. *Circulation* **1999**, *99* (19), 2503–2509. https://doi.org/10.1161/01.CIR.99.19.2503.
(16) Quillard, T.; Araújo, H. A.; Franck, G.; Tesmenitsky, Y.; Libby, P. Matrix Metalloproteinase-13 Predominates Over Matrix Metalloproteinase-8 as the Functional Interstitial Collagenase in Mouse Atheromata. *Arterioscler. Thromb. Vasc. Biol.* **2014**, *34* (6), 1179–1186. https://doi.org/10.1161/ATVBAHA.114.303326.
(17) Deguchi, J.-O.; Aikawa, E.; Libby, P.; Vachon, J. R.; Inada, M.; Krane, S. M.; Whittaker, P.; Aikawa, M. Matrix Metalloproteinase-13/Collagenase-3 Deletion Promotes Collagen Accumulation and Organization in Mouse Atherosclerotic Plaques. *Circulation* **2005**, *112* (17), 2708–2715. https://doi.org/10.1161/CIRCULATIONAHA.105.562041.
(18) Quillard, T.; Tesmenitsky, Y.; Croce, K.; Travers, R.; Shvartz, E.; Koskinas, K. C.; Sukhova, G. K.; Aikawa, E.; Aikawa, M.; Libby, P. Selective Inhibition of Matrix Metalloproteinase-13 Increases Collagen Content of Established Mouse Atherosclerosis. *Arterioscler. Thromb. Vasc. Biol.* **2011**, *31* (11), 2464–2472. https://doi.org/10.1161/ATVBAHA.111.231563.
(19) Cocker, M. S.; Spence, J. D.; Hammond, R.; deKemp, R. A.; Lum, C.; Wells, G.; Bernick, J.; Hill, A.; Nagpal, S.; Stotts, G.; Alturkustani, M.; Adeeko, A.; Yerofeyeva, Y.; Rayner, K.; Peterson, J.; Khan, A. R.; Naidas, A. C.; Garrard, L.; Yaffe, M. J.; Leung, E.; Prato, F. S.; Tardif, J.-C.; Beanlands, R. S. B. [18F]-Fluorodeoxyglucose PET/CT Imaging as a Marker of Carotid Plaque Inflammation: Comparison to Immunohistology and Relationship to Acuity of Events. *Int. J. Cardiol.* **2018**, *271*, 378–386. https://doi.org/10.1016/j.ijcard.2018.05.057.

(20) Tzolos, E.; Dweck, M. R. 18F-Sodium Fluoride (18F-NaF) for Imaging Microcalcification Activity in the Cardiovascular System. *Arterioscler. Thromb. Vasc. Biol.* **2020**, *40* (7), 1620–1626. https://doi.org/10.1161/atvbaha.120.313785.
(21) MacAskill, M. G.; Newby, D. E.; Tavares, A. A. S. Frontiers in Positron Emission Tomography Imaging of the Vulnerable Atherosclerotic Plaque. *Cardiovasc. Res.* **2019**, *115* (14), 1952–1962. https://doi.org/10.1093/cvr/cvz162.
(22) Toczek, J.; Ye, Y.; Gona, K.; Kim, H.-Y.; Han, J.; Razavian, M.; Golestani, R.; Zhang, J.; Wu, T. L.; Jung, J.-J.; Sadeghi, M. M. Preclinical Evaluation of RYM1, a Matrix Metalloproteinase-Targeted Tracer for Imaging Aneurysm. *J. Nucl. Med.* **2017**, *58* (8), 1318–1323. https://doi.org/10.2967/jnumed.116.188656.
(23) Ye, Y.; Toczek, J.; Gona, K.; Kim, H.-Y.; Han, J.; Razavian, M.; Golestani, R.; Zhang, J.; Wu, T. L.; Ghosh, M.; Jung, J.-J.; Sadeghi, M. M. Novel Arginine-Containing Macrocyclic MMP Inhibitors: Synthesis, 99mTc-Labeling, and Evaluation. *Sci. Rep.* **2018**, *8*, 11647. https://doi.org/10.1038/s41598-018-29941-2.
(24) Wagner, S.; Breyholz, H.-J.; Law, M. P.; Faust, A.; Höltke, C.; Schröer, S.; Haufe, G.; Levkau, B.; Schober, O.; Schäfers, M.; Kopka, K. Novel Fluorinated Derivatives of the Broad-Spectrum MMP Inhibitors N-Hydroxy-2(R)-[[(4-Methoxyphenyl)Sulfonyl](Benzyl)- and (3-Picolyl)-Amino]-3-Methyl-Butanamide as Potential Tools for the Molecular Imaging of Activated MMPs with PET. *J. Med. Chem.* **2007**, *50* (23), 5752–5764. https://doi.org/10.1021/jm0708533.
(25) Vazquez, N.; Missault, S.; Vangestel, C.; Deleye, S.; Thomae, D.; Veken, P. V. der; Augustyns, K.; Staelens, S.; Dedeurwaerdere, S.; Wyffels, L. Evaluation of [18F]BR420 and [18F]BR351 as Radiotracers for MMP-9 Imaging in Colorectal Cancer. *J. Label. Compd. Radiopharm.* **2017**, *60* (1), 69–79. https://doi.org/10.1002/jlcr.3476.
(26) Steward, W. P.; Thomas, A. L. Marimastat: The Clinical Development of a Matrix Metalloproteinase Inhibitor. *Expert Opin. Investig. Drugs* **2000**, *9* (12), 2913–2922. https://doi.org/10.1517/13543784.9.12.2913.
(27) Fields, G. B. The Rebirth of Matrix Metalloproteinase Inhibitors: Moving Beyond the Dogma. *Cells* **2019**, *8* (9), 984. https://doi.org/10.3390/cells8090984.
(28) Peterson, J. T. The Importance of Estimating the Therapeutic Index in the Development of Matrix Metalloproteinase Inhibitors. *Cardiovasc. Res.* **2006**, *69* (3), 677–687. https://doi.org/10.1016/j.cardiores.2005.11.032.
(29) Vandenbroucke, R. E.; Libert, C. Is There New Hope for Therapeutic Matrix Metalloproteinase Inhibition? *Nat. Rev. Drug Discov.* **2014**, *13* (12), 904–927. https://doi.org/10.1038/nrd4390.
(30) Hugenberg, V.; Wagner, S.; Kopka, K.; Schäfers, M.; Schuit, R. C.; Windhorst, A. D.; Hermann, S. Radiolabeled Selective Matrix Metalloproteinase 13 (MMP-13) Inhibitors: (Radio)Syntheses and in Vitro and First in Vivo Evaluation. *J. Med. Chem.* **2017**, *60* (1), 307–321. https://doi.org/10.1021/acs.jmedchem.6b01284.
(31) Engel, C. K.; Pirard, B.; Schimanski, S.; Kirsch, R.; Habermann, J.; Klingler, O.; Schlotte, V.; Weithmann, K. U.; Wendt, K. U. Structural Basis for the Highly Selective Inhibition of MMP-13. *Chem. Biol.* **2005**, *12* (2), 181–189. https://doi.org/10.1016/j.chembiol.2004.11.014.
(32) Nara, H.; Sato, K.; Naito, T.; Mototani, H.; Oki, H.; Yamamoto, Y.; Kuno, H.; Santou, T.; Kanzaki, N.; Terauchi, J.; Uchikawa, O.; Kori, M. Discovery of Novel, Highly Potent, and Selective Quinazoline-2-Carboxamide-Based Matrix Metalloproteinase (MMP)-13

Inhibitors without a Zinc Binding Group Using a Structure-Based Design Approach. *J. Med. Chem.* **2014**, *57* (21), 8886–8902. https://doi.org/10.1021/jm500981k.
(33) Nara, H.; Kaieda, A.; Sato, K.; Naito, T.; Mototani, H.; Oki, H.; Yamamoto, Y.; Kuno, H.; Santou, T.; Kanzaki, N.; Terauchi, J.; Uchikawa, O.; Kori, M. Discovery of Novel, Highly Potent, and Selective Matrix Metalloproteinase (MMP)-13 Inhibitors with a 1,2,4-Triazol-3-yl Moiety as a Zinc Binding Group Using a Structure-Based Design Approach. *J. Med. Chem.* **2017,** *60* (2), 608–626. https://doi.org/10.1021/acs.jmedchem.6b01007.
(34) Nara, H.; Sato, K.; Naito, T.; Mototani, H.; Oki, H.; Yamamoto, Y.; Kuno, H.; Santou, T.; Kanzaki, N.; Terauchi, J.; Uchikawa, O.; Kori, M. Thieno[2,3-d]Pyrimidine-2-Carboxamides Bearing a Carboxybenzene Group at 5-Position: Highly Potent, Selective, and Orally Available MMP-13 Inhibitors Interacting with the S1″ Binding Site. *Bioorg. Med. Chem.* **2014**, *22* (19), 5487–5505. https://doi.org/10.1016/j.bmc.2014.07.025.
(35) Choi, J. Y.; Fuerst, R.; Knapinska, A. M.; Taylor, A. B.; Smith, L.; Cao, X.; Hart, P. J.; Fields, G. B.; Roush, W. R. Structure-Based Design and Synthesis of Potent and Selective Matrix Metalloproteinase 13 Inhibitors. *J. Med. Chem.* **2017**, *60* (13), 5816–5825. https://doi.org/10.1021/acs.jmedchem.7b00514.
(36) Knapinska, A. M.; Singh, C.; Drotleff, G.; Blanco, D.; Chai, C.; Schwab, J.; Herd, A.; Fields, G. B. Matrix Metalloproteinase 13 Inhibitors for Modulation of Osteoclastogenesis: Enhancement of Solubility and Stability. *ChemMedChem* **2021**, *16* (7), 1133–1142. https://doi.org/10.1002/cmdc.202000911.
(37) Gege, C.; Bao, B.; Bluhm, H.; Boer, J.; Brian M. Gallagher, J.; Korniski, B.; Powers, T. S.; Steeneck, C.; Taveras, A. G.; Baragi, V. M. *Discovery and Evaluation of a Non-Zn Chelating, Selective Matrix Metalloproteinase 13 (MMP-13) Inhibitor for Potential Intra-articular Treatment of Osteoarthritis*. ACS Publications. https://doi.org/10.1021/jm201152u.
(38) Reiter, L. A.; Freeman-Cook, K. D.; Jones, C. S.; Martinelli, G. J.; Antipas, A. S.; Berliner, M. A.; Datta, K.; Downs, J. T.; Eskra, J. D.; Forman, M. D.; Greer, E. M.; Guzman, R.; Hardink, J. R.; Janat, F.; Keene, N. F.; Laird, E. R.; Liras, J. L.; Lopresti-Morrow, L. L.; Mitchell, P. G.; Pandit, J.; Robertson, D.; Sperger, D.; Vaughn-Bowser, M. L.; Waller, D. M.; Yocum, S. A. Potent, Selective Pyrimidinetrione-Based Inhibitors of MMP-13. *Bioorg. Med. Chem. Lett.* **2006**, *16* (22), 5822–5826. https://doi.org/10.1016/j.bmcl.2006.08.066.
(39) Ruminski, P. G.; Massa, M.; Strohbach, J.; Hanau, C. E.; Schmidt, M.; Scholten, J. A.; Fletcher, T. R.; Hamper, B. C.; Carroll, J. N.; Shieh, H. S.; Caspers, N.; Collins, B.; Grapperhaus, M.; Palmquist, K. E.; Collins, J.; Baldus, J. E.; Hitchcock, J.; Kleine, H. P.; Rogers, M. D.; McDonald, J.; Munie, G. E.; Messing, D. M.; Portolan, S.; Whiteley, L. O.; Sunyer, T.; Schnute, M. E. Discovery of N-(4-Fluoro-3-Methoxybenzyl)-6-(2-(((2S,5R)-5-(Hydroxymethyl)-1,4-Dioxan-2-Yl)Methyl)-2H-Tetrazol-5-Yl)-2-Methylpyrimidine-4-Carboxamide. A Highly Selective and Orally Bioavailable Matrix Metalloproteinase-13 Inhibitor for the Potential Treatment of Osteoarthritis. *J. Med. Chem.* **2016**, *59* (1), 313–327. https://doi.org/10.1021/acs.jmedchem.5b01434.
(40) Taylor, S. J.; Abeywardane, A.; Liang, S.; Xiong, Z.; Proudfoot, J. R.; Farmer, B. S.; Gao, D. A.; Heim-Riether, A.; Smith-Keenan, L. L.; Muegge, I.; Yu, Y.; Zhang, Q.; Souza, D.; Panzenbeck, M.; Goldberg, D.; Hill-Drzewi, M.; Margarit, M.; Collins, B.; Li, J. X.; Zuvela-Jelaska, L.; Li, J.; Farrow, N. A. Indole Inhibitors of MMP-13 for Arthritic Disorders. *ACS Omega* **2021**, *6* (29), 18635–18650. https://doi.org/10.1021/acsomega.1c01320.

(41) Buchler, A.; Munch, M.; Farber, G.; Zhao, X.; Al-Haddad, R.; Farber, E.; Rotstein, B. H. Selective Imaging of Matrix Metalloproteinase-13 to Detect Extracellular Matrix Remodeling in Atherosclerotic Lesions. *Mol. Imaging Biol.* **2021**. https://doi.org/10.1007/s11307-021-01626-9.
(42) Cai, H.; Agrawal, A. K.; Putt, D. A.; Hashim, M.; Reddy, A.; Brodfuehrer, J.; Surendran, N.; Lash, L. H. Assessment of the Renal Toxicity of Novel Anti-Inflammatory Compounds Using Cynomolgus Monkey and Human Kidney Cells. *Toxicology* **2009**, *258* (1), 56–63. https://doi.org/10.1016/j.tox.2009.01.006.
(43) Kreibich, M.; Petrović, D.; Brückner, R. Mechanistic Studies of the Deslongchamps Annulation. *J. Org. Chem.* **2018**, *83* (3), 1116–1133. https://doi.org/10.1021/acs.joc.7b02341.
(44) Bratteby, K.; Shalgunov, V.; Battisti, U. M.; Petersen, I. N.; van den Broek, S. L.; Ohlsson, T.; Gillings, N.; Erlandsson, M.; Herth, M. M. Insights into Elution of Anion Exchange Cartridges: Opening the Path toward Aliphatic 18F-Radiolabeling of Base-Sensitive Tracers. *ACS Pharmacol. Transl. Sci.* **2021**, *4* (5), 1556–1566. https://doi.org/10.1021/acsptsci.1c00133.
(45) Chen, J. M.; Nelson, F. C.; Levin, J. I.; Mobilio D.; Moy F. J.; Nilakantan R.; Zask, A.; Powers, R. Structure-Based Design of a Novel, Potent, and Selective Inhibitor for MMP-13 Utilizing NMR Spectroscopy and Computer-Aided Molecular Design. *J. Am. Chem. Soc.* **2000,** *122* (40), 9648–9654. https://doi.org/10.1021/ja001547g.
(46) Jaffré, F.; Friedman, A. E.; Hu, Z.; Mackman, N.; Blaxall, B. C. β-Adrenergic Receptor Stimulation Transactivates Protease-Activated Receptor 1 via Matrix Metalloproteinase 13 in Cardiac Cells. *Circulation* **2012**, *125* (24), 2993–3003. https://doi.org/10.1161/circulationaha.111.066787.
(47) Carretero, J. C.; García Ruano, J. L.; Vicioso, M. A Practical Route to C-8 Substituted Fluoroquinolones. *Tetrahedron* **1992**, *48* (35), 7373–7382. https://doi.org/10.1016/S0040-4020(01)88273-9.
(48) Neumann, U.; Kubota, H.; Frei, K.; Ganu, V.; Leppert, D. Characterization of Mca-Lys-Pro-Leu-Gly-Leu-Dpa-Ala-Arg-NH2, a Fluorogenic Substrate with Increased Specificity Constants for Collagenases and Tumor Necrosis Factor Converting Enzyme. *Anal. Biochem.* **2004**, *328* (2), 166–173. https://doi.org/10.1016/j.ab.2003.12.035.
(49) Wilson, A. A.; Jin, L.; Garcia, A.; DaSilva, J. N.; Houle, S. An Admonition When Measuring the Lipophilicity of Radiotracers Using Counting Techniques. *Appl. Radiat. Isot.* **2001**, *54* (2), 203–208. https://doi.org/10.1016/S0969-8043(00)00269-4.
(50) Andrés-Manzano, M. J.; Andrés, V.; Dorado, B. Oil Red O and Hematoxylin and Eosin Staining for Quantification of Atherosclerosis Burden in Mouse Aorta and Aortic Root. *Methods Mol. Biol. Clifton NJ* **2015**, *1339*, 85–99. https://doi.org/10.1007/978-1-4939-2929-0_5.